
Seasonal modeling analysis of nitrate formation pathways in Yangtze River Delta region, China

Jinjin Sun^{1,2}, Momei Qin^{1*}, Xiaodong Xie¹, Wenxing Fu¹, Yang Qin^{1,2}, Li Sheng¹, Lin Li¹, Jingyi Li¹, Ishaq Dimeji Sulaymon¹, Lei Jiang¹, Lin Huang¹, Xingna Yu², Jianlin Hu^{1*}

¹ Jiangsu Key Laboratory of Atmospheric Environment Monitoring and Pollution Control, Collaborative Innovation Center of Atmospheric Environment and Equipment Technology, Nanjing University of Information Science & Technology, Nanjing 210044, China

² Key Laboratory of Meteorological Disaster, Ministry of Education, Joint International Research Laboratory of Climate and Environment Change, Collaborative Innovation Center on Forecast and Evaluation of Meteorological Disasters, Key Laboratory for Aerosol-Cloud-Precipitation of China Meteorological Administration, Nanjing University of Information Science and Technology, Nanjing 210044, China

Correspondence to: Jianlin Hu (jianlinhu@nuist.edu.cn) and Momei Qin (momei.qin@nuist.edu.cn)

20

Abstract

Nitrate (NO_3^-) has been the dominant and the least reduced chemical component of fine particulate matter ($\text{PM}_{2.5}$) since the stringent emission control implemented in China in 2013. The formation pathways of NO_3^- vary seasonally and differ substantially in daytime vs. nighttime. They are affected by precursor emissions, atmospheric oxidation capacity, and meteorological conditions. Understanding NO_3^- formation pathways provides insights for the design of effective emission control strategies to mitigate NO_3^- pollution. In this study, the Community Multiscale Air Quality (CMAQ) model was applied to investigate the impact of regional transport, predominant physical processes, and different formation pathways to NO_3^- and total nitrate (TNO_3 , i.e., $\text{HNO}_3 + \text{NO}_3^-$) production in the Yangtze River Delta (YRD) region during the four seasons of 2017. $\text{NO}_3^-/\text{PM}_{2.5}$ and $\text{NO}_3^-/\text{TNO}_3$ are the highest in the winter, reaching 21% and 94%, respectively. Adjusted gas ratio ($\text{adjGR} = \frac{[\text{NH}_3] + [\text{NO}_3^-]}{[\text{HNO}_3] + [\text{NO}_3^-]}$) in the YRD is generally greater than two in different the four seasons across most areas in the YRD, indicating that YRD is mostly in the NH_3 -rich regime and NO_3^- is limited by HNO_3 formation. Local emissions and regional transportation contribute to YRD- NO_3^- concentrations throughout the YRD region by 50–62% and 38–50%, respectively. Majority of the regional transport of NO_3^- concentrations is contributed by indirect transport (i.e., NO_3^- formed by transported precursors reacting with local precursors). Aerosol (AERO, including condensation, coagulation, new particle formation and aerosol growth) processes are the dominant source of NO_3^- formation. In summer, NO_3^- formation is dominated by AERO and total transport (TRAN, sum of horizontal and vertical transport) processes. The $\text{OH} + \text{NO}_2$ pathway contributes to 60–83% of the TNO_3 production, and the N_2O_5 heterogeneous (HET N_2O_5) pathway contributes to 10–36% in the YRD region. HET N_2O_5 contribution becomes more important in cold seasons than warm seasons.

Within the planetary boundary layer in Shanghai, the TNO₃ production is dominated by the OH+NO₂ pathway during the day (98%) in the summer and spring, and by the HET N₂O₅ pathway during the night (61%) in the winter. Local contribution dominates the OH+NO₂ pathway for TNO₃ production during the day, while indirect transport dominates the HET N₂O₅ pathway at night.

Keywords: Nitrate formation pathways; chemical transport model, process analysis; local and transport contributions; Yangtze River Delta.

55 **1. Introduction**

The Yangtze River Delta (YRD) region, located in eastern China, is among the most populous and developed economic regions in China. Because of rapid population growth, economic advancement, urbanization, and industrialization during recent decades, the YRD region has been frequently suffering from both fine particulate matter (PM_{2.5}) and ozone (O₃) pollution problems (Qin et al., 2021; Sun et al., 2019; Dai et al., 2021). Particulate nitrate (NO₃⁻) is a major PM_{2.5} component and high concentrations of NO₃⁻ are often observed during cold seasons in the YRD region, due to high precursors emissions and regional transport contribution. Huang et al. (2014) reported that the daily average PM_{2.5} concentrations in Shanghai were 91 μg m⁻³ during haze pollution events of 5–25 January 2013, whereas NO₃⁻ accounted for 14% total PM_{2.5} mass. Huang et al. (2020a) observed that PM_{2.5} concentrations in Nanjing were 271 μg m⁻³ on 30–31 December of 2017, and the fraction of NO₃⁻ was ~27%. Lin et al. (2020) found that the peak concentration of NO₃⁻ in Nanjing was 85 μg m⁻³ during haze pollution events in the spring of 2016.

70 | Owing to the stringent emission control strategies ~~implemented in China~~ since 2013, primary PM_{2.5}, the major precursors (i.e., sulfur dioxide (SO₂) and nitrogen oxides (NO_x = nitric oxide (NO) + nitrogen dioxide (NO₂)) emissions have decreased

substantially in China, which led to significant decreases in primarytotal PM_{2.5} and sulfate (SO₄²⁻) mass concentrations ~~in China~~ (Li et al., 2022;Chen et al., 2021).

75 However, compared to SO₄²⁻ and other PM_{2.5} components, the reduction rate of NO₃⁻ was much less slower (Wen et al., 2018;Zhai et al., 2021;Zhou et al., 2022;Wang et al., 2022). This led to a rise in the ratio of NO₃⁻ mass to total PM_{2.5} in eastern China, rendering NO₃⁻ the dominant chemical component of PM_{2.5} (accounting for 24–35 %, especially during the cold season and haze pollution events) (Ding et al., 2019;Wen
80 et al., 2018;Lin et al., 2020;Fu et al., 2020;Zhou et al., 2022;Xie et al., 2022). High concentrations of NO₃⁻ influence the hygroscopicity and optical properties of particles, contributing to the formation of haze and to visibility degradation (Hu et al., 2021;Xie et al., 2020). Mitigating NO₃⁻ pollution has become an urgent concern in the YRD.

85 NO₃⁻ is formed in the atmosphere by a series of chemical reactions leading to the production of nitric acid (HNO₃) and then following gas-to-particle partitioning (Griffith et al., 2015;Guo et al., 2018;Lin et al., 2020). The key NO₃⁻ formation pathways include the gas-phase oxidation (hydroxyl (OH) and NO₂) and the heterogeneous hydrolysis of dinitrogen a dinitrogen pentoxide (HET N₂O₅) on the
90 wet particles' surface (Fan et al., 2021;Wang et al., 2018;Chen et al., 2020). ~~Several studies investigated the importance of different pathways to NO₃⁻ formation in various locations using~~The chemical transport models (CTMs), field observations, ~~the~~ box model, ~~or~~ as well as oxygen and nitrogen isotope techniques apply to quantify the contribution of different pathways to NO₃⁻ formation in various locations. For
95 example, He et al. (2020) and Li et al. (2021b) reported that the OH+NO₂ pathway dominates daytime NO₃⁻ formation in the YRD, accounting for 60–92 % and 55–86 % in warm and cold seasons, respectively. The HET N₂O₅ pathway is the main nocturnal-NO₃⁻ formation in winter, especially in severe haze episodes, with contributions of 44–97 % at night (Fu et al., 2020;He et al., 2018). Furthermore, Tan

100 et al. (2021) and Wang et al. (2018) indicated that the chemical formation cannot explain the variation of TNO₃ at the surface (sum of NO₃⁻ and HNO₃), due to the concentrations of N₂O₅ being close to zero and controlled by high NO emissions at night. Fan et al. (2021) and Kim et al. (2014) further emphasized the contributions of NO₃⁻ formation pathways differ significantly at vertical altitudes, owing to the
105 vertical gradients of nocturnal NO₃ and total oxidant (NO₂+O₃) level within the planetary boundary layer (PBL). Prabhakar et al. (2017) revealed that the active nocturnal NO₃⁻ formation ~~via the HET-N₂O₅ pathway~~ from the upper PBL contributed 80 % to daytime surface NO₃⁻ concentrations in winter of 2013 in California,~~accounting for 80 %.~~

110 The complex NO₃⁻ formation chemistry involves the anthropogenic emission of precursors (i.e., NO_x, and ammonia (NH₃)) and atmospheric oxidants (i.e., OH, O₃, and ~~N₂O₅~~NO₃) (Chan et al., 2021;Womack et al., 2019). ~~Studies~~Previous studies suggested that NO₃⁻ responds nonlinearly to its precursors emissions reductions in major Chinese regions (i.e., the North China Plain (NCP) and YRD), emphasizing
115 that the uncoordinated control of precursors (i.e., SO₂, NH₃, and NO_x) increase the atmospheric oxidant capacity (AOC) and enhance NO₃⁻ formation in NO_x-rich regimes (Li et al., 2021b;Huang et al., 2020b;Lu et al., 2021a). Coupled with the chemical formation, regional transport also plays important roles in NO₃⁻ pollution formation. Previous modeling studies using the CTMs highlighted the important role
120 of the regional transport in NO₃⁻ concentrations in major regions of eastern China (Itahashi et al., 2017;Qu et al., 2021;Ying et al., 2014;Shen et al., 2020). For example, Huang et al. (2020a) reported that secondary pollutants are regionally transported between the NCP and YRD regions (a distance of 1000 km), and hence simultaneously exacerbate the levels of secondary inorganic aerosols (SIA) in two
125 major Chinese regions. Ying et al. (2014) revealed that the regional air pollution transport from the north and central China contributed about 45 % to NO₃⁻ in

Shanghai during the winter of 2009. Wu et al. (2017) suggested that the regional transport plays a key role in NO_3^- sources in Shanghai (accounting for about 90 %), while local emission only contributed 10 % for NO_3^- in January 2013. ~~Shen et al. (2020)~~ Shen et al. (2020) reported that the contribution of regional transport amounted to around 60–98 % to the high concentrations of NO_3^- under severe haze episodes in two winters of 2015 and 2016 in the YRD. Qu et al. (2021) found that the indirect transport made a contribution of 43 % to NO_3^- in the Pearl River Delta (PRD) region in cold season of 2015, mainly due to chemical reactions between the locally emitted NO_x and transported O_3 at night. Du et al. (2020) also revealed that regional transport contributed about 56 % to NO_3^- in Beijing in winter 2017, mainly produced via indirect transport.

The NO_3^- ~~formation~~chemical pathways and ~~formation~~controlling factors ~~can~~may be very different in different seasons ~~even~~in the same studying ~~region~~locations. Most previous studies ~~on~~ NO_3^- have focused on ~~one or only~~a few short period of NO_3^- pollution episodes, ~~but lack of~~and lacked the seasonal analysis ~~for the full year~~. This study aims to obtain a comprehensive understanding of the seasonal variations in the NO_3^- formation mechanisms, as well as to determine key precursors, dominant processes and chemical pathways in ~~the~~YRD. The Community Multiscale Air Quality (CMAQ) model was employed to investigate the contributions of various physical and chemical processes to NO_3^- and HNO_3 formation. Regional transport and chemical reaction pathways were quantified for the YRD region. The analyses were conducted in the four seasons of 2017 to compare and identify the key impact factors for NO_3^- in different seasons, and to provide a scientific basis for designing effective emissions control strategies to mitigate the urgent NO_3^- pollution in the YRD region.

2. Methods

2.1. Model configuration

The CMAQ v5.2 model (Wyat Appel et al., 2018;Liu et al., 2020b;Sheng et al.,
155 2022) was applied to investigate the major chemical pathways and physical processes
that contribute to NO_3^- and TNO_3 formation in the YRD region. Two nested domains
were used, as shown in Fig. 1. The outer domain (36 km horizontal resolution)
spanned eastern and southeastern China, while the inner domain (12 km horizontal
resolution) spanned the entire YRD region. The simulation periods were January,
160 April, July, and October 2017, representing the winter, spring, summer, and autumn,
respectively. The simulation began three days prior to each of the study periods, and
the results were not included in the model analysis as they served as a spin-up of the
model.

The CMAQ model was configured using the photochemical mechanism of the
165 State-wide Air Pollution Research Center version 07 (SAPRC07tic) and the
sixth-generation aerosol (AERO6i) module (Fu et al., 2020;Sulaymon et al., 2021).
Further details about the CMAQ modeling system provided in previous studies (Hu et
al., 2016;Liu et al., 2020b). The Weather Research and Forecasting model (WRF v4.2,
<http://www.wrf-model.org>) was used to simulate the required meteorological fields
170 inputs, with initial and boundary meteorological conditions from the $1^\circ \times 1^\circ$ National
Centers for Environmental Prediction Final (NCEP/FNL) reanalysis data
(<https://rda.ucar.edu/datasets/ds083.2/>). ~~Detailed~~The detailed configurations of the
WRF model ~~provided shown in the studies of Table S1, consistent with~~ Hu et al. (2016)
and Wang et al. (2021), ~~shown in Table S1,.~~ The anthropogenic emissions ~~offor the~~
175 2017 ~~in the~~ YRD region were ~~released~~established by the Shanghai Academy of
Environmental Sciences (SAES), a high-resolution (4 km × 4 km) anthropogenic
emission inventory across the entire YRD region (An et al., 2021), ~~and used for the
entire YRD region.~~ The Multi-resolution Emission Inventory for China of the year

2017 with resolution of $0.25^\circ \times 0.25^\circ$ (MEIC v1.3, <http://meicmodel.org>) served as
180 the anthropogenic emissions for other Chinese regions outside the YRD (Zheng et al.,
2018). Emissions from other regions outside China in the inner domain were
calculated using the gridded Regional Emission inventory in ASia (REAS v3.2, 0.25°
 $\times 0.25^\circ$ resolution) emissions of the year 2015. The global model of emissions of
gases and aerosols from nature (MEGAN v2.1) was used to estimate biogenic
185 emissions (Guenther et al., 2012). Biomass burning emissions were based on satellite
observations including both gases and aerosols from the 2017 Fire Inventory from
NCAR (FINN) (Wiedinmyer et al., 2011). Further descriptions of the emissions
processing are provided in previous studies by Hu et al. (2016) and Qiao et al. (2015),
and therefore not repeated here.

190 2.2. Contributions of transport

To quantify the contributions of local and regional transport to the surface
concentrations of the nitrate-phase species (i.e., HNO_3 and NO_3^-), four scenarios were
simulated under the same meteorological fields. Briefly, in the first (base) scenario,
the anthropogenic emissions of 2017 in the YRD and outside regions were included.
195 In the second (YRD-zero) scenario, anthropogenic emissions in the YRD were set to
zero, while anthropogenic emissions in regions outside YRD were used. In the third
(outside-zero) scenario, only anthropogenic emissions in the YRD were included,
while the regions outside the YRD were set to zero. The fourth (all-zero) scenario
represented the background case, where the anthropogenic emissions within the study
200 domain were set to zero.

The predicted concentrations were denoted as C_{base} , $C_{\text{YRD-zero}}$, $C_{\text{outside-zero}}$, and
 $C_{\text{all-zero}}$, representing ~~concentration~~ NO_3^- concentrations associated with the base,
YRD-zero, outside-zero, and all-zero scenarios, respectively. ~~For NO_3^- in YRD, the~~
The contributions of local YRD emissions, regional transport (the sum of direct and
205 indirect transport from outside regions), direct transport (NO_3^- contributed by

transported precursors from outside regions), indirect transport (NO_3^- contributed by transported and local-emitted precursors via the OH+NO₂ and HET N₂O₅ chemical pathway), and background were defined as F_{Local} , F_{Region} , F_{Direct} , F_{Indirect} , and $F_{\text{Background}}$, and they were quantified/calculated as follows:

$$210 \quad F_{\text{Local}} = (C_{\text{outside-zero}} - C_{\text{all-zero}})/C_{\text{base}} \quad (1)$$

$$F_{\text{Region}} = (C_{\text{base}} - C_{\text{outside-zero}})/C_{\text{base}} \quad (2)$$

$$F_{\text{Direct}} = (C_{\text{YRD-zero}} - C_{\text{all-zero}})/C_{\text{base}} \quad (23)$$

$$F_{\text{Indirect}} = [(C_{\text{base}} - C_{\text{outside-zero}}) - (C_{\text{YRD-zero}} - C_{\text{all-zero}})]/C_{\text{base}} \quad (34)$$

$$F_{\text{Background}} = C_{\text{all-zero}}/C_{\text{base}} \quad (45)$$

215 ~~In addition to~~ Besides NO_3^- , the major gases pollutants (i.e., O_3 , NH_3 , NO_2 , and HNO_3), atmospheric oxidants (i.e., OH, O₃ and N₂O₅) OH, and particulate pollutants (i.e., PM_{2.5}, SO₄²⁻, and SOCTNO₃) were also quantified. The values of the contributions of the local, direct and indirect transport emissions can be greater or less than zero, which represents the generation or depletion of pollutants through chemical reactions between local and non-local precursors.

220

2.3. Process analysis

In the CMAQ model system, the process analysis (PA) tool has two components, including the Integrated Process Rate (IPR) and Integrated Reaction Rate (IRR) (Liu et al., 2011; Byun and Schere, 2006). The IPR analysis was applied to investigate the cumulative effect of chemical and physical processes to NO_3^- and HNO_3 formation and their daily variation within the PBL (Chen et al., 2019; Yang et al., 2020; Kim et al., 2014). These processes, as explained in Table S2, include aerosol processes (AERO), gas chemistry (CHEM), emission (EMIS), horizontal transport (HTRA), vertical transport (VTRA), dry deposition (DDEP), and cloud processes (CLDS). Furthermore, the IRR analysis was employed to quantify the rates of TNO₃ chemical reactions pathways (Qu et al., 2021; Fu et al., 2020; Shen et al., 2020). The complex chemical

230

production of TNO_3 involves eight reactions pathways, detailed in Table S3 (Qu et al., 2021;Fu et al., 2020;Chuang et al., 2022). In the latter analyses, these pathways are grouped into three major TNO_3 production pathways, including the $\text{OH}+\text{NO}_2$, HET N_2O_5 , and “Others” pathways, according to their importance. Shanghai is selected as an example in the IPR and IRR analysis to explore the impacts of physical and chemical processes of NO_3^- and HNO_3 formation because it is the largest city in the YRD and has the most abundant measurement data.

2.4. Observation data

Hourly concentrations of six routine air pollutants (i.e., O_3 , $\text{PM}_{2.5}$, NO_2 , SO_2 , and carbon monoxide (CO)) in five representative YRD cities (i.e., Shanghai, Nanjing, Hefei, Hangzhou, and Changzhou, shown in Fig. 1) during the four seasons were obtained from the China Ministry of Ecology and Environment (<http://106.37.208.233:20035/>, last accessed on April 30, 2022). Furthermore, hourly NO_3^- concentrations were measured by the Monitors for AeRosols and Gases (MARGA 1S ADI 2080, Netherlands) (Khezri et al., 2013) at four urban atmospheric environment supersites, including Shanghai (31.23 °N, 121.54 °E), Hefei (31.78 °N, 117.20 °E), Hangzhou (30.29 °N, 120.16 °E), and Changzhou (31.76 °N, 119.96 °E). Observation data of meteorological parameters (temperature (T_2 , °C), relative humidity (RH, %), wind speed (WS, m/s) and wind direction (WD, °)) for 75 weather stations in the YRD were downloaded from the Chinese Meteorological Agency (<http://data.cma.cn/en>, last accessed on November 30, 2021).

The statistical metrics used for the WRF-CMAQ model evaluation include the mean bias (MB), normalized mean bias (NMB), normalized mean error (NME), correlation coefficient (R), root mean square error (RMSE), and index of agreement (IOA). Definitions and criteria of all statistical metrics are illustrated in Table S4. The benchmarks of major air pollutants ($\text{PM}_{2.5}$, NO_2 , O_3 , and NO_3^-) concentrations are suggested by Emery et al. (2017) and Huang et al. (2021). The benchmarks of major

meteorological parameters (T2, WS, and WD) are suggested by Emery and Tai
260 (2001).

3. Results and discussion

3.1. Model evaluation

3.1.1. WRF model performance

Table 1 shows the modeling performance statistics of the meteorological
265 parameters in the four seasons of 2017. Predicted T2 and WS values are slightly
higher than the observations, and MB values of T2 and WS exceed the suggested
benchmark ($MB \leq \pm 0.5$) in all seasons. The seasonal and annual IOA values of T2
occur within the suggested benchmark ($IOA \geq 0.8$). For WS, the seasonal and annual
values of RMSE and IOA all meet the suggested criterion ($RMSE \leq 2.0$ and $IOA \geq$
270 0.6). The MB values of WD are slightly above the suggested benchmark ($MB \leq \pm 10$)
in the four seasons, except during spring. RH is generally under-estimated compared
to the observations with averaged MB values of -6.96 , -10.7 , -9.06 , and -5.98 in
winter, spring, summer, and autumn, respectively. No suggested criterion for MB
value of RH. In addition, high seasonal and annual values of R (0.85 – 0.95 for T;
275 0.87 – 0.91 for RH; 0.70 – 0.85 for WS; and 0.75 – 0.89 for WD) are found. The WRF
performance in this study is comparable to WRF performance in [our](#) previous
[simulation](#) studies (Wang et al., 2021; Hu et al., 2016; Sulaymon et al., 2021).

3.1.2. CMAQ model performance

Table 2 and Fig. S1 show the model performance and time series of major air
280 pollutants in the four seasons. Overall, the CMAQ model has reasonably reproduced
the observed $PM_{2.5}$, O_3 , and NO_2 concentrations in the YRD region, especially in
Shanghai. The daily concentrations of $PM_{2.5}$ are efficiently simulated in the five cities
except Hefei, illustrated by the NMB, NME, and R values meeting the criteria
established by Emery et al. (2017) ($NMB \leq \pm 0.30$, $NME \leq 0.50$, and $R > 0.70$).

285 MDA8 O₃ are slightly overestimated in Nanjing, Hefei, Hangzhou, and Changzhou.
Predicted concentrations of NO₂ are generally lower than the observations in all five
cities ($-0.15 < \text{NMB} \leq -0.05$, $-10.37 < \text{MB} \leq -1.89$). When compared to our previous
~~air-quality-simulation~~ studies (Hu et al., 2016; Wang et al., 2021; Ma et al.,
2021; Sulaymon et al., 2021; Li et al., 2021a), the statistical results in this study show a
290 better model performance.

Fig. 2 illustrates the comparison of predicted and observed NO₃⁻ concentrations
at the four supersites on daily timescales (~~Fig. S2 shows the hourly predicted and
observed NO₃⁻ concentrations~~). The general temporal variations of observed NO₃⁻
concentrations are efficiently captured by the model. The daily concentrations of NO₃⁻
295 are efficiently predicted in four supersites, all within the benchmark (NMB ≤ ±0.60,
NME ≤ 0.75, and R > 0.6). But in Hefei (Fig. 2b), the wintertime NO₃⁻ measurement
data is not available, when NO₃⁻ shows the highest concentrations and is of most
concern. Good agreement between predicted and observed values is demonstrated on
daily timescales, especially in Shanghai (NMB = -0.49, R = 0.70), Hangzhou (NMB
300 = 0.11, MB = 0.64) and Changzhou (NMB = 0.36, R = 0.56). ~~The seasonal daily
concentrations of NO₃⁻ are efficiently predicted in Shanghai, Hangzhou and
Changzhou, within the benchmark (NMB ≤ ±0.60, NME ≤ 0.75, and R > 0.6).~~
The Overall, the performance statistical metrics of predicted NO₃⁻ in this study are
comparable to those of our previous studies works (Shi et al., 2017; Qu et al., 2021; Xie
305 et al., 2022). Fig. S2 shows the hourly predicted and observed NO₃⁻ concentrations in
each season. NO₃⁻ concentrations are generally underestimated during the summer and
autumn. One possible reason is that RH is slightly underestimated by the WRF model
during these seasons (Table 1), which results in a lower buildup of NO₃⁻
concentrations. Other reasons could be associated with uncertainties in the NO₃⁻
310 formation mechanisms (~~i.e., missing or insufficient heterogeneous reactions~~) in the
current CMAQ model) and uncertainties in NO_x and NH₃ emissions (Zheng et al.,

2020;Lu et al., 2021b;Zheng et al., 2015;Liu et al., 2019;Xie et al., 2022).

3.2. Regional transport contribution to nitrate in YRD

Fig. S3 shows the spatial distribution of the seasonal (winter, spring, summer and autumn) and annual ~~mean~~ (average of the four seasons) NO_3^- , HNO_3 , and TNO_3 concentrations under four ~~different~~ emissions scenarios in the d02 domain. Under C_{base} , the seasonal and annual ~~predicted~~ NO_3^- concentrations ~~of~~ NO_3^- for the entire YRD region were 16.0, 7.4, 1.0, 5.4, and 7.4 $\mu\text{g m}^{-3}$, respectively (Table S5). Compared to C_{base} , the seasonal and annual ~~YRD~~ NO_3^- concentrations in $C_{\text{outside-zero}}$ decreased by 8.0, 2.8, 0.4, 2.2, and 3.3 $\mu\text{g m}^{-3}$, respectively. Even more significant differences in NO_3^- are observed between C_{base} and $C_{\text{YRD-zero}}$. The NO_3^- ~~values~~ decreased by 12.0, 6.9, 0.9, 4.8 and 6.1 $\mu\text{g m}^{-3}$ in winter, spring, summer, autumn, and ~~the~~ year, respectively, to become almost twice as high as those between C_{base} and $C_{\text{outside-zero}}$. The results suggest that the ~~YRD~~ local anthropogenic emissions contribute more to the seasonal NO_3^- concentrations ~~in the YRD~~.

Fig. 3 shows the regional contributions of the background, local, direct and indirect transport to nitrate-related species in the four seasons (results for Shanghai are shown in Fig S5S4). The local emissions dominate NO_3^- concentrations throughout the YRD ~~NO_3^-~~ , accounting for 50.4–62.0 % in the four seasons (Fig. 3a). Fig 3c suggests that the precursors (NO_2 and NH_3) are dominated by the local emissions (more than 93.0%). The contributions of the total regional transport (~~sum of indirect and direct transport~~) are 49.5, 38.0, 41.6, and 42.0 % in winter, spring, summer, and autumn, respectively. The indirect transport contributes 24.2–37.0% of NO_3^- concentrations, and exceeds the contributions from direct transport in the spring, summer, and autumn. Similarly, Qu et al. (2021) reported that the reaction between the locally emitted NO_x and transported O_3 dominates the production of indirect NO_3^- transport in the PRD region.

In Fig. 3b, the local emission and indirect transport have negative contributions

to O₃ concentration, leading to the depletion of O₃ in the four seasons. ~~The~~ For O₃, the local emissions have negative contribution ~~to O₃~~ in winter (~~-45.646%~~) and autumn (~~-12.3%~~), ~~and %~~). ~~The negative contributions of~~ the indirect transport ~~has negative contribution~~ are ~~-6, -8, -8, and -4 %~~ in ~~winter, spring~~ (~~-8.5%~~), ~~summer~~, and autumn (~~-8.7%~~). ~~For O₃ and OH~~ (~~, respectively~~). In Fig. 3b and 3d), ~~the~~ indirect transport contributes ~~about 8% and from -42% to -12%~~ ~~—42%—~~ of OH concentrations in ~~all the four~~ seasons, ~~respectively~~. The negative indirect transport contributions to O₃, N₂O₅, and OH suggest that the atmospheric oxidants are consumed in the YRD, which in turn enhances the chemical production of NO₃⁻.

3.3. Formation processes of nitrate

Fig. 4 shows the modeled diurnal variations of three nitrate-phases (NO₃⁻, HNO₃, and TNO₃), the major precursors (i.e., O₃, NO₂, and NH₃), and the major atmospheric oxidants (OH and N₂O₅) in the four seasons for the entire YRD region in the base scenario. Except for summer, higher predicted TNO₃ and NO₃⁻ concentrations are observed in early morning hours (6:00–8:00 am), while lower TNO₃ and NO₃⁻ concentrations are observed around 16:00–18:00 pm. Predicted concentrations of TNO₃, HNO₃, and O₃ show the same diurnal variations in the summer, and peak around 12:00 pm (the most active photochemical hours). The opposite profiles of TNO₃'s diurnal variation between summer and non-summer are mainly attributed to the temperature effect on the gas-to-particle partitioning between NO₃⁻ and HNO₃. As shown in Fig. S3, NO₃⁻ dominates the TNO₃ concentrations and determines its diurnal variations in non-summer, while HNO₃ dominates the diurnal variation in summer. A two-peak mode diurnal variation of NO₂ and NH₃ is identified in the four seasons. High concentrations of NO₂ and NH₃ occur in the early morning (hours 6:00–8:00 am) and early evening (hours 18:00-19:00 pm), due to the local transportation emissions during rush hours. OH and N₂O₅ have a one-peak mode diurnal variation in the four seasons. OH peaks around 12:00 pm, similar to HNO₃, while N₂O₅ peaks around

18:00–20:00 pm.

Fig. ~~S7S6~~ shows seasonal variations in $\text{NO}_3^-/\text{PM}_{2.5}$, $\text{NO}_3^-/\text{TNO}_3$, nitrogen oxidation ratios ($\text{NOR} = [\text{NO}_3^-]/([\text{NO}_3^-] + [\text{NO}_2])$), and adjusted gas ratio ($\text{adjGR} = ([\text{NH}_3] + [\text{NO}_3^-])/([\text{HNO}_3] + [\text{NO}_3^-])$) in the YRD. $\text{NO}_3^-/\text{PM}_{2.5}$ and $\text{NO}_3^-/\text{TNO}_3$ are the highest in the winter, accounting for $21 \pm 5\%$ and $94 \pm 3\%$, respectively. The averaged NOR values for the entire YRD region are 0.24, 0.16, 0.03, and 0.13 mol/mol in winter, spring, summer, and autumn, respectively. The highest value of NOR in winter suggests a high conversion efficiency of NO_2 to NO_3^- . AdjGR values are generally greater than two in the four seasons across most areas in the YRD, indicating that YRD is mostly in the NH_3 -rich regime. Therefore, NH_3 is not a limiting factor of NO_3^- formation in YRD.

~~Shanghai is selected as the example city in the IPRs analysis to explore the impacts of physical and chemical processes of NO_3^- and HNO_3 formation within the PBL.~~ Fig. 5 illustrates a two-peak mode diurnal variation of the net IPRs rates of NO_3^- production in the four seasons. Peak hours are around mid-noon (10:00–11:00 am) and early evening (19:00–21:00 pm), with peak rates of 1.2–1.5, 0.7–0.8, 0.4–0.6, and 0.1–0.2 $\mu\text{g m}^{-3} \text{h}^{-1}$ in the winter, spring, summer, and autumn, respectively. AERO processes (including condensation, coagulation, and aerosol growth) are the dominant contributors of NO_3^- formation, with the peak rates of 2.1, 1.3, 1.5, and 0.4 $\mu\text{g m}^{-3} \text{h}^{-1}$ in the winter, spring, summer, and autumn, respectively. The sharp decline hours of the net IPRs (around 11:00–18:00 pm) are mainly dominated by TRAN (sum of HTRA and VTRA) processes, with the mean rates of -1.4 , -0.8 , -0.7 , and $-0.3 \mu\text{g m}^{-3} \text{h}^{-1}$ in the winter, spring, summer, and autumn, respectively. However, in summer, TRAN processes constitute the dominant source during midnight (1:00–6:00 am), owing to higher the stable PBL weakening the contribution of vertical transport and accelerating the accumulation of NO_3^- concentrations at the upper PBL contributing to the surface through the vertical mixing and development of the PBL (Huang et al.,

2020c). In Fig. S9S7, VTRA processes act as the main positive contributor to NO_3^- buildup production from 0:00 to 23:00 at layer 1 (surface layer), while AERO processes make the negative contribution to NO_3^- within layers 1–8 (from the surface to 800 m). Above layer 10, AERO processes for NO_3^- production are positive in the daytime, which is conducive to the accumulation of NO_3^- concentrations.

For HNO_3 , a one-peak mode diurnal variation of the net IPRs rates is found, and peak times are at 20:00 pm in the winter and around 9:00–12:00 am in other seasons (Fig. 5). Meanwhile, CHEM (gas chemical processes) processes are the major contributor to HNO_3 formation, with the peak rates being 0.6, 1.4, 2.3, and 0.7 ppb h^{-1} in the winter, spring, summer, and autumn, respectively. In the spring, summer and autumn, the peak times of HNO_3 formation are consistent with the first-peak times of NO_3^- . The seasonal net IPRs rates reached a maximum of 0.3, 1.0, and 0.1 ppb h^{-1} , respectively. CHEM and VTRA processes are the dominant contributors of HNO_3^- production, especially during 7:00 to 13:00 (net IPRs rates > 0), with the seasonal peak rates of 1.5, 2.7, and 0.8 ppb h^{-1} , respectively. AERO, DDEP, and HTRA processes are the dominant contributors of the HNO_3^- sharp decline (14:00–17:00 pm), with the lowest net IPRs rates of -0.8 , -0.7 , and $-0.3 \mu\text{g m}^{-3} \text{h}^{-1}$ in the spring, summer, and autumn, respectively. DDEP processes are the dominant sink of HNO_3 in summer ($-0.64 \pm 0.20 \text{ ppb h}^{-1}$). However, in the winter, the peak times of HNO_3 production are opposite with the first-peak time of NO_3^- production, but consistent with the second-peak time. HTRA make a positive contribution to HNO_3^- with peak rates of 0.18 ppb h^{-1} at 20:00 pm. In Fig. S12, the only-largest sink is the AERO process, consistent with efficient partitioning of HNO_3 into particle phase NO_3^- in cold seasons.

Table 3 illustrates that within the PBL, in cold seasons (winter and autumn), about 60–78 % of TNO_3 is produced through $\text{OH}+\text{NO}_2$, 21–36 % through HET N_2O_5 , and 2–5 % through the “Others” pathways in the five representative YRD cities.

420 Meanwhile, 71–83 % of TNO₃ is produced through OH+NO₂, 10–23 % through HET
N₂O₅, and 4–13 % through the “Others” pathways (mainly contributed by NO₃+Org
and N₂O₅ H₂O) in warm seasons (summer and spring). Table 4 shows the comparison
of the contribution of the major TNO₃ production pathways studies in China and other
regions using different methods. The results are in agreement with the contribution of
425 NO₃⁻ pathways in previous modeling and observational studies. For example, Li et al.
(2021b) modeled that OH+NO₂ and HET N₂O₅ pathways dominate NO₃⁻ production
in the YRD region in warm and cold seasons of 2016 by the CTM, accounting for 86–
92 % and 8–14 % in the surface layer, respectively. He et al. (2020) reported that the
OH+NO₂ pathway dominates NO₃⁻ production in Shanghai on the surface layer using
430 nitrogen isotopes analysis, accounting for 84–92 % and 55–77 % in the warm and
cold seasons of 2016, respectively. Alexander et al. (2020) highlighted that the
OH+NO₂ and HET N₂O₅ pathways contribute the same proportion (both 41 % in the
four seasons) to NO₃⁻ production in the global region using the CTM and oxygen
isotopes analysis.

435 Fig. 6a shows the diurnal variations of TNO₃ formation reactions rates through
three major pathways in Shanghai within the PBL. The average diurnal trends of
TNO₃ production rates are consistent with the CHEM processes rates of HNO₃
production (Figs. 5–6). The chemical production of HNO₃ quickly transforms to
particulate NO₃⁻, through AERO processes in the presence of abundant NH₃. ~~In the~~
440 ~~winter, spring, summer, and autumn, the~~The averaged TNO₃ production rates are 0.31
± 0.14, 0.65 ± 0.37, 1.09 ± 0.68, and 0.28 ± 0.22 ppb h⁻¹, ~~in the winter, spring,~~
~~summer, and autumn,~~ respectively (Table S6). Moreover, the seasonal peak rates of
TNO₃ production are 0.6, 1.4, 2.3, and 0.7 ppb h⁻¹ around 11:00 am –13:00 pm,
respectively. In accordance with the seasonal variation of HNO₃ net IPRs rates, TNO₃
445 production rates are the fastest in summer.

In Shanghai, TNO₃ chemical production is dominated by the OH+NO₂ pathway

on the daily timescale, accounting for 69.3–86.9 % of the total, while the HET N₂O₅ pathway is likewise a relatively important pathway (accounting for 11.1–28.4 %) in the four seasons (Fig. 6b). Notably, TNO₃ production rates are dominated by the OH+NO₂ pathway during the daytime (7:00 am–18:00 pm, accounting for 88.4–97.9 % of the total) in all seasons, while the HET N₂O₅ pathway becomes more important for the TNO₃ production during the nighttime (19:00 pm – 06:00 am, accounting for 42.5–61.6%). During winter, TNO₃ formation via the HET N₂O₅ pathway becomes dominant over the OH+NO₂ pathway, accounting for 62, 65, and 68% in Shanghai, Hangzhou and Nanjing at night, respectively. O₃ strongly coordinates TNO₃ production ~~in YRD~~ via the HET N₂O₅ pathway during the nighttime. Similarly, He et al. (2018) observed that the HET N₂O₅ pathway was the major contributor to NO₃⁻ production in the winter of Beijing at the surface layer, using oxygen and nitrogen isotopes analysis, accounting for 56–97 % of the total during the nighttime. In another CTM study in the NCP, the HET N₂O₅ pathway was the dominant contributor to nocturnal-NO₃⁻ production within the PBL in winter, with a contribution of 83 % at night (Liu et al., 2020a). In Fig. S8, the seasonal TNO₃ production rates (ppb/h) and contributions (%) of the major pathways have been compared between vertical layers and PBL. The OH+NO₂ pathway dominated TNO₃ production at all layers, accounting for more than 58%, 78%, 80%, and 83% in winter, spring, summer, and autumn, respectively. The OH+NO₂ pathway rate decreases with altitude at vertically layers, where its contribution decreases from 87% to 58%, from 91% to 78%, from 93% to 80%, and from 95% to 83% in the four seasons, respectively. The HET N₂O₅ pathway becomes more important for the TNO₃ production within layers 4~8 (250 to 580 m) in winter, accounting for 37% (Fig. S8b).

Fig. 7 displays the contributions of TNO₃ formation pathways from the local and transport (sum of indirect and direct transport) contributions. For the local contribution, the averaged TNO₃ production rates are 0.27 ± 0.14 , 0.56 ± 0.37 , $1.05 \pm$

0.69, and 0.26 ± 0.21 ppb h⁻¹ in the winter, spring, summer, and autumn, respectively
475 (Table [S8S7](#)). During the daytime, the OH+NO₂ pathway contributes almost all TNO₃
production rates from the local contribution, accounting for about 89–98 % of the
total, with mean rates of 0.33 ± 0.17 , 0.83 ± 0.34 , 1.55 ± 0.59 , and 0.40 ± 0.22 ppb h⁻¹
in the winter, spring, summer, and autumn, respectively. The results suggest that the
locally-emitted NO₂ reacts with ~~locally-formed~~ OH dominated TNO₃ production rates
480 during the day in the ~~urban~~-YRD region.

For the transport contribution, the averaged TNO₃ production rates are $0.04 \pm$
 0.01 , 0.08 ± 0.02 , 0.03 ± 0.02 , and 0.02 ± 0.01 ppb h⁻¹ in the winter, spring, summer,
and autumn, respectively (Table [S9S8](#)). The HET N₂O₅ pathway is noted as the
dominant pathway for TNO₃ production of the transport contribution, accounting for
485 around 72–86 % during the nighttime. Fig. [7b8](#) compares the seasonal TNO₃
production pathways rates between local, indirect and direct transport contributions.
within the PBL. The regional production is mainly contributed by indirect transport,
especially in the winter and summer. The results suggest that the transported O₃ from
outside YRD region ~~can~~ react with the locally-emitted NO₂, supporting ~~HNO₃~~
490 ~~formation~~TNO₃ production via the HET N₂O₅ ~~chemistry~~chemical pathway ~~at~~
~~night~~during the nighttime.

Overall, our findings illustrate that local emissions dominate NO₃⁻ formation in
the YRD (50–62%), more specifically, locally-emitted NO_x reacting with OH and
partitioning into particles with NH₃ (mostly from local sources, more than 93.0%),
495 indicating that the uncoordinated control of precursors (i.e., NO_x and NH₃) and
reduction of the oxidative capacity of the atmosphere is crucial for NO₃⁻ reduction.
Furthermore, regional transport contributes 38–50% to NO₃⁻ formation in the YRD
region. Indirect transport contributes 24–37% through transported O₃ reacting with
local NO_x at night, indicating that the simultaneous controlling of O₃ and NO₃⁻ in the
500 larger scale region is also important for NO₃⁻ reduction in the YRD.

This manuscript investigated the seasonal variations in the NO_3^- formation mechanisms, including local emission and regional transport contributions, as well as dominant processes and major chemical pathways in the YRD region. However, there are still some limitations in this manuscript, such as the insufficient heterogeneous chemistry on the dust particles' surface and uncertainties in precursors emissions in the model affect the model performance of NO_3^- during the spring and autumn (Xie et al., 2022). Furthermore, the Integrated Reaction Rate (IRR) analysis was employed to quantify the rates of TNO_3 (sum of NO_3^- and HNO_3) chemical pathways, which potentially lead to differences in chemical pathways rates and contributions between NO_3^- and TNO_3 . Figure 6(b) illustrates that TNO_3 chemical production is dominated by the $\text{OH}+\text{NO}_2$ pathway on the daily timescale, accounting for 69.3–86.9 % in Shanghai. Notably, due to the higher temperature during the daytime, the potential production for NO_3^- is not as high as that of the nocturnal chemical pathway (mainly the HET N_2O_5 pathway at night), which potentially lead to underestimate in the nocturnal pathway contribution to NO_3^- .

4. Conclusions

This study investigates the contributions of regional transport and major chemical pathways to the of NO_3^- and HNO_3 formation in the YRD in different seasons using the WRF-CMAQ model. The modeled results show that local emissions dominate ~~YRD-regional~~ NO_3^- concentrations in the YRD (50–62%), while regional transport contributes 38–50% to NO_3^- (indirect transport contributes 24–37%). Except for winter, HNO_3 was dominated by the contributions of local emissions (61–75%) and indirect transport contributed negatively –24 to –41%. In Shanghai, the IPRs analysis reveals that AERO processes were the predominant contributors in NO_3^- formation within the PBL. TRAN processes were the largest sinks in NO_3^- formation in the winter, spring and autumn, while the positive contributors at night in summer.

For HNO₃, CHEM processes were the only positive contributor during the day. The OH+NO₂ pathway is the predominant contributor (60–83%) among all chemical pathways, while the HET N₂O₅ pathway is also important (10–36%) in the YRD region. The TNO₃ production is dominated by the OH+NO₂ pathway during the day (98%) in summer, while the HET N₂O₅ pathway dominates during the night (61%) in winter. The TNO₃ production rates from the local and transport contributions were further elucidated. The OH+NO₂ pathway from the local contribution strongly dominates the TNO₃ production during the day (89–98%). At night, the HET N₂O₅ pathway mainly dominates by indirect transport (via reaction with transported O₃ at night).

Code and data availability

Hourly concentrations of O₃, PM_{2.5}, NO₂, SO₂, and CO used in this study are freely available through the website of <http://106.37.208.233:20035/> (last accessed on April 30, 2022). Observation data of meteorological parameters used in this study are available from <http://data.cma.cn/en> (last accessed on November 30, 2021). The CMAQ outputs are currently available upon request, all python codes used to create any of the figures are available upon request.

Author contributions

JS, MQ and JH designed research. JS, MQ, XX, WF, YQ, LS, and LL contributed to model development, simulations, and data processing. JL, IS, LJ, LH, XY contributed to result discussion. JS prepared the manuscript and all coauthors helped improve the manuscript.

Competing interests

The authors declare that they have no conflict of interest.

555 Acknowledgements

This work was supported by the National Natural Science Foundation of China (42007187, 92044302, 42021004), and the Postgraduate Research & Practice Innovation Program of Jiangsu Province (KYCX21_0954).

References

- 560 Alexander, B., Sherwen, T., Holmes, C. D., Fisher, J. A., Chen, Q., Evans, M. J., and Kasibhatla, P.: Global inorganic nitrate production mechanisms: comparison of a global model with nitrate isotope observations, *Atmos. Chem. Phys.*, 20, 3859-3877, 10.5194/acp-20-3859-2020, 2020.
- An, J., Huang, Y., Huang, C., Wang, X., Yan, R., Wang, Q., Wang, H., Jing, S., Zhang, Y., Liu, Y., Chen, Y., Xu, C., Qiao, L., Zhou, M., Zhu, S., Hu, Q., Lu, J., and Chen, C.: Emission inventory of air pollutants and chemical speciation for specific anthropogenic sources based on local measurements in the Yangtze River Delta region, China, *Atmos. Chem. Phys.*, 21, 2003-2025, 10.5194/acp-21-2003-2021, 2021.
- Byun, D., and Schere, K. L.: Review of the Governing Equations, Computational Algorithms, and Other Components of the Models-3 Community Multiscale Air Quality (CMAQ) Modeling System, *ApMRv*, 59, 51-77, 10.1115/1.2128636, 2006.
- 570 Chan, Y.-C., Evans, M. J., He, P., Holmes, C. D., Jaeglé L., Kasibhatla, P., Liu, X.-Y., Sherwen, T., Thornton, J. A., Wang, X., Xie, Z., Zhai, S., and Alexander, B.: Heterogeneous Nitrate Production Mechanisms in Intense Haze Events in the North China Plain, *Journal of Geophysical Research: Atmospheres*, 126, e2021JD034688, <https://doi.org/10.1029/2021JD034688>, 2021.
- 575 Chen, T.-F., Chang, K.-H., and Lee, C.-H.: Simulation and analysis of causes of a haze episode by combining CMAQ-IPR and brute force source sensitivity method, *Atmos. Environ.*, 218, 117006, <https://doi.org/10.1016/j.atmosenv.2019.117006>, 2019.
- Chen, X., Jiang, Z., Shen, Y., Li, R., Fu, Y., Liu, J., Han, H., Liao, H., Cheng, X., Jones, D. B. A., Worden, H., and Abad, G. G.: Chinese Regulations Are Working—Why Is Surface Ozone Over
- 580 Industrialized Areas Still High? Applying Lessons From Northeast US Air Quality Evolution, *Geophys. Res. Lett.*, 48, e2021GL092816, <https://doi.org/10.1029/2021GL092816>, 2021.
- Chen, X. R., Wang, H. C., Lu, K. D., Li, C., Zhai, T., Tan, Z., Ma, X., Yang, X., Liu, Y., Chen, S., Dong, H., Li, X., Wu, Z., Hu, M., Zeng, L., and Zhang, Y.: Field Determination of Nitrate Formation Pathway in Winter Beijing, *Environ. Sci. Technol.*, 54, 9243-9253, 10.1021/acs.est.0c00972, 2020.

- 585 Chuang, M.-T., Wu, C.-F., Lin, C.-Y., Lin, W.-C., Chou, C. C. K., Lee, C.-T., Lin, T.-H., Fu, J. S., and Kong, S. S.-K.: Simulating nitrate formation mechanisms during PM_{2.5} events in Taiwan and their implications for the controlling direction, *Atmos. Environ.*, 269, 118856, <https://doi.org/10.1016/j.atmosenv.2021.118856>, 2022.
- 590 Dai, H. B., Zhu, J., Liao, H., Li, J., Liang, M., Yang, Y., and Yue, X.: Co-occurrence of ozone and PM_{2.5} pollution in the Yangtze River Delta over 2013–2019: Spatiotemporal distribution and meteorological conditions, *Atmos. Res.*, 249, 105363, <https://doi.org/10.1016/j.atmosres.2020.105363>, 2021.
- Ding, A. J., Huang, X., Nie, W., Chi, X., Xu, Z., Zheng, L., Xu, Z., Xie, Y., Qi, X., Shen, Y., Sun, P., Wang, J., Wang, L., Sun, J., Yang, X. Q., Qin, W., Zhang, X., Cheng, W., Liu, W., Pan, L., and Fu, C.: Significant reduction of PM_{2.5} in eastern China due to regional-scale emission control: evidence from SORPES in 2011–2018, *Atmos. Chem. Phys.*, 19, 11791–11801, 10.5194/acp-19-11791-2019, 2019.
- 595 Du, H., Li, J., Wang, Z., Dao, X., Guo, S., Wang, L., Ma, S., Wu, J., Yang, W., Chen, X., and Sun, Y.: Effects of Regional Transport on Haze in the North China Plain: Transport of Precursors or Secondary Inorganic Aerosols, *Geophys. Res. Lett.*, 47, e2020GL087461, 10.1029/2020gl087461, 2020.
- 600 Emery, C., and Tai, E.: Enhanced Meteorological Modeling and Performance Evaluation for Two Texas Ozone Episodes, Final Report Submitted to Texas Natural Resources Conservation Commission, 2001.
- Emery, C., Liu, Z., Russell, A. G., Odman, M. T., Yarwood, G., and Kumar, N.: Recommendations on statistics and benchmarks to assess photochemical model performance, *J. Air Waste Manage. Assoc.*, 67, 582–598, 10.1080/10962247.2016.1265027, 2017.
- 605 Fan, M.-Y., Zhang, Y.-L., Lin, Y.-C., Cao, F., Zhao, Z.-Y., Sun, Y., Qiu, Y., Fu, P., and Wang, Y.: Changes of Emission Sources to Nitrate Aerosols in Beijing After the Clean Air Actions: Evidence From Dual Isotope Compositions, *Journal of Geophysical Research: Atmospheres*, 125, e2019JD031998, 10.1029/2019JD031998, 2020.
- Fan, M.-Y., Zhang, Y.-L., Lin, Y.-C., Hong, Y., Zhao, Z.-Y., Xie, F., Du, W., Cao, F., Sun, Y., and Fu, P.: Important Role of NO₃ Radical to Nitrate Formation Aloft in Urban Beijing: Insights from Triple Oxygen Isotopes Measured at the Tower, *Environ. Sci. Technol.*, 10.1021/acs.est.1c02843, 2021.
- 610 Fu, X., Wang, T., Gao, J., Wang, P., Liu, Y., Wang, S., Zhao, B., and Xue, L.: Persistent Heavy Winter Nitrate Pollution Driven by Increased Photochemical Oxidants in Northern China, *Environ. Sci. Technol.*, 54, 3881–3889, 10.1021/acs.est.9b07248, 2020.
- 615 Griffith, S. M., Huang, X. H. H., Louie, P. K. K., and Yu, J. Z.: Characterizing the thermodynamic and chemical composition factors controlling PM_{2.5} nitrate: Insights gained from two years of online measurements in Hong Kong, *Atmos. Environ.*, 122, 864–875, <https://doi.org/10.1016/j.atmosenv.2015.02.009>, 2015.
- 620 Guenther, A. B., Jiang, X., Heald, C. L., Sakulyanontvittaya, T., Duhl, T., Emmons, L. K., and Wang, X.: The Model of Emissions of Gases and Aerosols from Nature version 2.1 (MEGAN2.1): an extended and updated framework for modeling biogenic emissions, *Geosci. Model Dev.*, 5, 1471–1492, 10.5194/gmd-5-1471-2012, 2012.
- Guo, H., Otjes, R., Schlag, P., Kiendler-Scharr, A., Nenes, A., and Weber, R. J.: Effectiveness of ammonia reduction on control of fine particle nitrate, *Atmos. Chem. Phys.*, 18, 12241–12256, 10.5194/acp-18-12241-2018, 2018.
- 625 He, P., Xie, Z., Chi, X., Yu, X., Fan, S., Kang, H., Liu, C., and Zhan, H.: Atmospheric $\Delta^{17}\text{O}(\text{NO}_3^-)$ reveals nocturnal chemistry dominates nitrate production in Beijing haze, *Atmos. Chem. Phys.*, 18, 14465–14476, 10.5194/acp-18-14465-2018, 2018.

-
- 630 He, P., Xie, Z., Yu, X., Wang, L., Kang, H., and Yue, F.: The observation of isotopic compositions of atmospheric nitrate in Shanghai China and its implication for reactive nitrogen chemistry, *Sci. Total Environ.*, 714, 136727, <https://doi.org/10.1016/j.scitotenv.2020.136727>, 2020.
- Hu, J., Chen, J., Ying, Q., and Zhang, H.: One-year simulation of ozone and particulate matter in China using WRF/CMAQ modeling system, *Atmos. Chem. Phys.*, 16, 10333-10350, 10.5194/acp-16-10333-2016, 2016.
- 635 Hu, S., Zhao, G., Tan, T., Li, C., Zong, T., Xu, N., Zhu, W., and Hu, M.: Current challenges of improving visibility due to increasing nitrate fraction in PM_{2.5} during the haze days in Beijing, China, *Environ. Pollut.*, 290, 118032, <https://doi.org/10.1016/j.envpol.2021.118032>, 2021.
- Huang, L., Zhu, Y., Zhai, H., Xue, S., Zhu, T., Shao, Y., Liu, Z., Emery, C., Yarwood, G., Wang, Y., Fu, J., Zhang, K., and Li, L.: Recommendations on benchmarks for numerical air quality model applications in China – Part 1: PM_{2.5} and chemical species, *Atmos. Chem. Phys.*, 21, 2725-2743, 10.5194/acp-21-2725-2021, 2021.
- 640 Huang, R. J., Zhang, Y. L., Bozzetti, C., Ho, K.-F., Cao, J.-J., Han, Y., Daellenbach, K. R., Slowik, J. G., Platt, S. M., Canonaco, F., Zotter, P., Wolf, R., Pieber, S. M., Bruns, E. A., Crippa, M., Ciarelli, G., Piazzalunga, A., Schwikowski, M., Abbazade, G., Schnelle-Kreis, J., Zimmermann, R., An, Z., Szidat, S., Baltensperger, U., Haddad, I. E., and Prévôt, A. S. H.: High secondary aerosol contribution to particulate pollution during haze events in China, *Nature*, 514, 218-222, 10.1038/nature13774, 2014.
- 645 Huang, X., Ding, A., Wang, Z., Ding, K., Gao, J., Chai, F., and Fu, C.: Amplified transboundary transport of haze by aerosol–boundary layer interaction in China, *Nat. Geosci.*, 13, 428-434, 10.1038/s41561-020-0583-4, 2020a.
- 650 Huang, X., Ding, A. J., Gao, J., Zheng, B., Zhou, D., Qi, X., Tang, R., Wang, J., Ren, C., Nie, W., Chi, X., Xu, Z., Chen, L., Li, Y., Che, F., Pang, N., Wang, H., Tong, D., Qin, W., Cheng, W., Liu, W., Fu, Q., Liu, B., Chai, F., Davis, S. J., Zhang, Q., and He, K.: Enhanced secondary pollution offset reduction of primary emissions during COVID-19 lockdown in China, *Natl. Sci. Rev.*, 8, nwaa137, 10.1093/nsr/nwaa137, 2020b.
- 655 Huang, X., Huang, J. T., Ren, C. H., Wang, J., Wang, H., Wang, J., Yu, H., Chen, J., Gao, J., and Ding, A.: Chemical Boundary Layer and Its Impact on Air Pollution in Northern China, *Environ. Sci. Technol. Lett.*, 10.1021/acs.estlett.0c00755, 2020c.
- Itahashi, S., Uno, I., Osada, K., Kamiguchi, Y., Yamamoto, S., Tamura, K., Wang, Z., Kurosaki, Y., and Kanaya, Y.: Nitrate transboundary heavy pollution over East Asia in winter, *Atmos. Chem. Phys.*, 17, 3823-3843, 10.5194/acp-17-3823-2017, 2017.
- 660 Khezri, B., Mo, H., Yan, Z., Chong, S.-L., Heng, A. K., and Webster, R. D.: Simultaneous online monitoring of inorganic compounds in aerosols and gases in an industrialized area, *Atmos. Environ.*, 80, 352-360, <https://doi.org/10.1016/j.atmosenv.2013.08.008>, 2013.
- Kim, Y. J., Spak, S. N., Carmichael, G. R., Riemer, N., and Stanier, C. O.: Modeled aerosol nitrate formation pathways during wintertime in the Great Lakes region of North America, *Journal of Geophysical Research: Atmospheres*, 119, 412,420-412,445, <https://doi.org/10.1002/2014JD022320>, 2014.
- 665 Li, C., Hammer, M. S., Zheng, B., and Cohen, R. C.: Accelerated reduction of air pollutants in China, 2017-2020, *Sci. Total Environ.*, 803, 150011, <https://doi.org/10.1016/j.scitotenv.2021.150011>, 2022.
- 670 Li, L., Xie, F., Li, J., Gong, K., Xie, X., Qin, Y., Qin, M., and Hu, J.: Diagnostic analysis of regional ozone pollution in Yangtze River Delta, China: A case study in summer 2020, *Sci. Total Environ.*, 151511, <https://doi.org/10.1016/j.scitotenv.2021.151511>, 2021a.

-
- Li, M., Zhang, Z., Yao, Q., Wang, T., Xie, M., Li, S., Zhuang, B., and Han, Y.: Nonlinear responses of particulate nitrate to NO_x emission controls in the megalopolises of China, *Atmos. Chem. Phys.*, 21, 15135-15152, 10.5194/acp-21-15135-2021, 2021b.
- 675 Lin, Y. C., Zhang, Y. L., Fan, M. Y., and Bao, M.: Heterogeneous formation of particulate nitrate under ammonium-rich regimes during the high-PM_{2.5} events in Nanjing, China, *Atmos. Chem. Phys.*, 20, 3999-4011, 10.5194/acp-20-3999-2020, 2020.
- Liu, L., Liu, L., Liu, S., Li, X., Zhou, J., Feng, T., Cao, J., Qian, Y., Cao, J., and Li, G.: Effects of organic coating on the nitrate formation by suppressing the N₂O₅ heterogeneous hydrolysis: A case study during wintertime in Beijing-Tianjin-Hebei (BTH), *Atmos. Chem. Phys.*, 19, 8189-8207, 10.5194/acp-19-8189-2019, 2019.
- 680 Liu, L., Bei, N., Hu, B., Wu, J., Liu, S., Li, X., Wang, R., Liu, Z., Shen, Z., and Li, G.: Wintertime nitrate formation pathways in the north China plain: Importance of N₂O₅ heterogeneous hydrolysis, *Environ. Pollut.*, 266, 115287, <https://doi.org/10.1016/j.envpol.2020.115287>, 2020a.
- 685 Liu, P., Zhang, Y., Yu, S., and Schere, K. L.: Use of a process analysis tool for diagnostic study on fine particulate matter predictions in the U.S.–Part II: Analyses and sensitivity simulations, *Atmospheric Pollution Research*, 2, 61-71, <https://doi.org/10.5094/APR.2011.008>, 2011.
- Liu, T., Wang, X. Y., Hu, J. L., Wang, Q., An, J., Gong, K., Sun, J., Li, L., Qin, M., Li, J., Tian, J., Huang, Y., Liao, H., Zhou, M., Hu, Q., Yan, R., Wang, H., and Huang, C.: Driving Forces of Changes in Air Quality during the COVID-19 Lockdown Period in the Yangtze River Delta Region, China, *Environ. Sci. Technol. Lett.*, 7, 779-786, 10.1021/acs.estlett.0c00511, 2020b.
- 690 Lu, M., Tang, X., Feng, Y., Wang, Z., Chen, X., Kong, L., Ji, D., Liu, Z., Liu, K., Wu, H., Liang, S., Zhou, H., and Hu, K.: Nonlinear response of SIA to emission changes and chemical processes over eastern and central China during a heavy haze month, *Sci. Total Environ.*, 788, 147747, <https://doi.org/10.1016/j.scitotenv.2021.147747>, 2021a.
- 695 Lu, X., Ye, X., Zhou, M., Zhao, Y., Weng, H., Kong, H., Li, K., Gao, M., Zheng, B., Lin, J., Zhou, F., Zhang, Q., Wu, D., Zhang, L., and Zhang, Y.: The underappreciated role of agricultural soil nitrogen oxide emissions in ozone pollution regulation in North China, *Nature Communications*, 12, 5021, 10.1038/s41467-021-25147-9, 2021b.
- 700 Luo, L., Kao, S., Wu, Y., Zhang, X., Lin, H., Zhang, R., and Xiao, H.: Stable oxygen isotope constraints on nitrate formation in Beijing in springtime, *Environ. Pollut.*, 263, 114515, <https://doi.org/10.1016/j.envpol.2020.114515>, 2020a.
- Luo, L., Pan, Y.-Y., Zhu, R.-G., Zhang, Z.-Y., Zheng, N.-J., Liu, Y.-H., Liu, C., Xiao, H.-W., and Xiao, H.-Y.: Assessment of the seasonal cycle of nitrate in PM_{2.5} using chemical compositions and stable nitrogen and oxygen isotopes at Nanchang, China, *Atmos. Environ.*, 225, 117371, <https://doi.org/10.1016/j.atmosenv.2020.117371>, 2020b.
- 705 Ma, J., Shen, J., Wang, P., Zhu, S., Wang, Y., Wang, P., Wang, G., Chen, J., and Zhang, H.: Modeled changes in source contributions of particulate matter during the COVID-19 pandemic in the Yangtze River Delta, China, *Atmos. Chem. Phys.*, 21, 7343-7355, 10.5194/acp-21-7343-2021, 2021.
- 710 Prabhakar, G., Parworth, C. L., Zhang, X., Kim, H., Young, D. E., Beyersdorf, A. J., Ziemba, L. D., Nowak, J. B., Bertram, T. H., Faloona, I. C., Zhang, Q., and Cappa, C. D.: Observational assessment of the role of nocturnal residual-layer chemistry in determining daytime surface particulate nitrate concentrations, *Atmos. Chem. Phys.*, 17, 14747-14770, 10.5194/acp-17-14747-2017, 2017.
- 715 Qiao, X., Tang, Y., Hu, J., Zhang, S., Li, J., Kota, S. H., Wu, L., Gao, H., Zhang, H., and Ying, Q.: Modeling dry and wet deposition of sulfate, nitrate, and ammonium ions in Jiuzhaigou National Nature

- Reserve, China using a source-oriented CMAQ model: Part I. Base case model results, *Sci. Total Environ.*, 532, 831-839, <https://doi.org/10.1016/j.scitotenv.2015.05.108>, 2015.
- 720 Qin, Y., Li, J. Y., Gong, K. J., Wu, Z., Chen, M., Qin, M., Huang, L., and Hu, J.: Double high pollution events in the Yangtze River Delta from 2015 to 2019: Characteristics, trends, and meteorological situations, *Sci. Total Environ.*, 792, 148349, <https://doi.org/10.1016/j.scitotenv.2021.148349>, 2021.
- 725 Qu, K., Wang, X. S., Xiao, T., Shen, J., Lin, T., Chen, D., He, L.-Y., Huang, X.-F., Zeng, L., Lu, K., Ou, Y., and Zhang, Y.: Cross-regional transport of PM_{2.5} nitrate in the Pearl River Delta, China: Contributions and mechanisms, *Sci. Total Environ.*, 753, 142439, <https://doi.org/10.1016/j.scitotenv.2020.142439>, 2021.
- 730 Shah, V., Jaeglé L., Thornton, J. A., Lopez-Hilfiker, F. D., Lee, B. H., Schroder, J. C., Campuzano-Jost, P., Jimenez, J. L., Guo, H., Sullivan, A. P., Weber, R. J., Green, J. R., Fiddler, M. N., Bililign, S., Campos, T. L., Stell, M., Weinheimer, A. J., Montzka, D. D., and Brown, S. S.: Chemical feedbacks weaken the wintertime response of particulate sulfate and nitrate to emissions reductions over the eastern United States, *Proceedings of the National Academy of Sciences*, 115, 8110-8115, [10.1073/pnas.1803295115](https://doi.org/10.1073/pnas.1803295115), 2018.
- 735 Shen, J., Zhao, Q., Cheng, Z., Wang, P., Ying, Q., Liu, J., Duan, Y., and Fu, Q.: Insights into source origins and formation mechanisms of nitrate during winter haze episodes in the Yangtze River Delta, *Sci. Total Environ.*, 741, 140187, [10.1016/j.scitotenv.2020.140187](https://doi.org/10.1016/j.scitotenv.2020.140187), 2020.
- 740 Sheng, L., Qin, M., Li, L., Wang, C., Gong, K., Liu, T., Li, J., and Hu, J.: Impacts of emissions along the lower Yangtze River on air quality and public health in the Yangtze River delta, China, *Atmospheric Pollution Research*, 101420, <https://doi.org/10.1016/j.apr.2022.101420>, 2022.
- 745 Shi, Z., Li, J., Huang, L., Wang, P., Wu, L., Ying, Q., Zhang, H., Lu, L., Liu, X., Liao, H., and Hu, J.: Source apportionment of fine particulate matter in China in 2013 using a source-oriented chemical transport model, *Sci. Total Environ.*, 601-602, 1476-1487, <https://doi.org/10.1016/j.scitotenv.2017.06.019>, 2017.
- 750 Sulaymon, I. D., Zhang, Y., Hu, J., Hopke, P. K., Zhang, Y., Zhao, B., Xing, J., Li, L., and Mei, X.: Evaluation of regional transport of PM_{2.5} during severe atmospheric pollution episodes in the western Yangtze River Delta, China, *J. Environ. Manage.*, 293, 112827, <https://doi.org/10.1016/j.jenvman.2021.112827>, 2021.
- 755 Sun, J. J., Liang, M. J., Shi, Z. H., Shen, F., Li, J., Huang, L., Ge, X., Chen, Q., Sun, Y., Zhang, Y., Chang, Y., Ji, D., Ying, Q., Zhang, H., Kota, S. H., and Hu, J.: Investigating the PM_{2.5} mass concentration growth processes during 2013–2016 in Beijing and Shanghai, *Chemosphere*, 221, 452-463, <https://doi.org/10.1016/j.chemosphere.2018.12.200>, 2019.
- 760 Sun, P., Nie, W., Chi, X., Xie, Y., Huang, X., Xu, Z., Qi, X., Xu, Z., Wang, L., Wang, T., Zhang, Q., and Ding, A.: Two years of online measurement of fine particulate nitrate in the western Yangtze River Delta: influences of thermodynamics and N₂O₅ hydrolysis, *Atmos. Chem. Phys.*, 18, 17177-17190, [10.5194/acp-18-17177-2018](https://doi.org/10.5194/acp-18-17177-2018), 2018.
- 765 Tan, Z. F., Wang, H. C., Lu, K. D., Dong, H. B., Liu, Y. H., Zeng, L. M., Hu, M., and Zhang, Y. H.: An Observational Based Modeling of the Surface Layer Particulate Nitrate in the North China Plain During Summertime, *J Geophys Res-Atmos*, 126, e2021JD035623, ARTN e2021JD035623 [10.1029/2021JD035623](https://doi.org/10.1029/2021JD035623), 2021.
- 770 Vrekoussis, M., Kanakidou, M., Mihalopoulos, N., Crutzen, P. J., Lelieveld, J., Perner, D., Berresheim, H., and Baboukas, E.: Role of the NO₃ radicals in oxidation processes in the eastern Mediterranean troposphere during the MINOS campaign, *Atmos. Chem. Phys.*, 4, 169-182,

-
- 10.5194/acp-4-169-2004, 2004.
- Wang, H., Lu, K., Chen, X., Zhu, Q., Wu, Z., Wu, Y., and Sun, K.: Fast particulate nitrate formation via N₂O₅ uptake aloft in winter in Beijing, *Atmos. Chem. Phys.*, 18, 10483-10495, 10.5194/acp-18-10483-2018, 2018.
- 765 Wang, J., Gao, J., Che, F., Wang, Y., Lin, P., and Zhang, Y.: Decade-long trends in chemical component properties of PM_{2.5} in Beijing, China (2011–2020), *Sci. Total Environ.*, 154664, <https://doi.org/10.1016/j.scitotenv.2022.154664>, 2022.
- Wang, X., Li, L., Gong, K., Mao, J., Hu, J., Li, J., Liu, Z., Liao, H., Qiu, W., Yu, Y., Dong, H., Guo, S., Hu, M., Zeng, L., and Zhang, Y.: Modelling air quality during the EXPLORE-YRD campaign – Part I.
- 770 Model performance evaluation and impacts of meteorological inputs and grid resolutions, *Atmos. Environ.*, 246, 118131, <https://doi.org/10.1016/j.atmosenv.2020.118131>, 2021.
- Wang, Y.-L., Song, W., Yang, W., Sun, X.-C., Tong, Y.-D., Wang, X.-M., Liu, C.-Q., Bai, Z.-P., and Liu, X.-Y.: Influences of Atmospheric Pollution on the Contributions of Major Oxidation Pathways to PM_{2.5} Nitrate Formation in Beijing, *Journal of Geophysical Research: Atmospheres*, 124, 4174-4185, <https://doi.org/10.1029/2019JD030284>, 2019.
- 775 Wen, L., Xue, L., Wang, X., Xu, C., Chen, T., Yang, L., Wang, T., Zhang, Q., and Wang, W.: Summertime fine particulate nitrate pollution in the North China Plain: increasing trends, formation mechanisms and implications for control policy, *Atmos. Chem. Phys.*, 18, 11261-11275, 10.5194/acp-18-11261-2018, 2018.
- 780 Wiedinmyer, C., Akagi, S. K., Yokelson, R. J., Emmons, L. K., Al-Saadi, J. A., Orlando, J. J., and Soja, A. J.: The Fire INventory from NCAR (FINN): a high resolution global model to estimate the emissions from open burning, *Geosci. Model Dev.*, 4, 625-641, 10.5194/gmd-4-625-2011, 2011.
- Womack, C. C., McDuffie, E. E., Edwards, P. M., Bares, R., de Gouw, J. A., Docherty, K. S., Dubé W. P., Fibiger, D. L., Franchin, A., Gilman, J. B., Goldberger, L., Lee, B. H., Lin, J. C., Long, R., Middlebrook, A. M., Millet, D. B., Moravek, A., Murphy, J. G., Quinn, P. K., Riedel, T. P., Roberts, J. M., Thornton, J. A., Valin, L. C., Veres, P. R., Whitehill, A. R., Wild, R. J., Warneke, C., Yuan, B., Baasandorj, M., and Brown, S. S.: An Odd Oxygen Framework for Wintertime Ammonium Nitrate Aerosol Pollution in Urban Areas: NO_x and VOC Control as Mitigation Strategies, *Geophys. Res. Lett.*, 46, 4971-4979, <https://doi.org/10.1029/2019GL082028>, 2019.
- 785 Wu, C., Liu, L., Wang, G., Zhang, S., Li, G., Lv, S., Li, J., Wang, F., Meng, J., and Zeng, Y.: Important contribution of N₂O₅ hydrolysis to the daytime nitrate in Xi'an, China during haze periods: Isotopic analysis and WRF-Chem model simulation, *Environ. Pollut.*, 288, 117712, <https://doi.org/10.1016/j.envpol.2021.117712>, 2021.
- 790 Wu, J.-B., Wang, Z., Wang, Q., Li, J., Xu, J., Chen, H., Ge, B., Zhou, G., and Chang, L.: Development of an on-line source-tagged model for sulfate, nitrate and ammonium: A modeling study for highly polluted periods in Shanghai, China, *Environ. Pollut.*, 221, 168-179, <https://doi.org/10.1016/j.envpol.2016.11.061>, 2017.
- 795 Wyatt Appel, K., Napelenok, S., Hogrefe, C., Pouliot, G., Foley, K. M., Roselle, S. J., Pleim, J. E., Bash, J., Pye, H. O. T., Heath, N., Murphy, B., and Mathur, R.: Overview and Evaluation of the Community Multiscale Air Quality (CMAQ) Modeling System Version 5.2, *Air Pollution Modeling and its Application XXV*, Cham, 2018, 69-73.
- 800 Xie, X., Hu, J., Qin, M., Guo, S., Hu, M., Wang, H., Lou, S., Li, J., Sun, J., Li, X., Sheng, L., Zhu, J., Chen, G., Yin, J., Fu, W., Huang, C., and Zhang, Y.: Modeling particulate nitrate in China: current findings and future directions, *Environ. Int.*, 107369, <https://doi.org/10.1016/j.envint.2022.107369>,

- 805 2022.
Xie, Y., Wang, G., Wang, X., Chen, J., Chen, Y., Tang, G., Wang, L., Ge, S., Xue, G., Wang, Y., and Gao, J.: Nitrate-dominated PM_{2.5} and elevation of particle pH observed in urban Beijing during the winter of 2017, *Atmos. Chem. Phys.*, 20, 5019-5033, 10.5194/acp-20-5019-2020, 2020.
- 810 Yang, X., Wu, K., Wang, H., Liu, Y., Gu, S., Lu, Y., Zhang, X., Hu, Y., Ou, Y., Wang, S., and Wang, Z.: Summertime ozone pollution in Sichuan Basin, China: Meteorological conditions, sources and process analysis, *Atmos. Environ.*, 226, 117392, <https://doi.org/10.1016/j.atmosenv.2020.117392>, 2020.
- Ying, Q., Wu, L., and Zhang, H.: Local and inter-regional contributions to PM_{2.5} nitrate and sulfate in China, *Atmos. Environ.*, 94, 582-592, <https://doi.org/10.1016/j.atmosenv.2014.05.078>, 2014.
- 815 Zang, H., Zhao, Y., Huo, J., Zhao, Q., Fu, Q., Duan, Y., Shao, J., Huang, C., An, J., Xue, L., Li, Z., Li, C., and Xiao, H.: High atmospheric oxidation capacity drives wintertime nitrate pollution in the eastern Yangtze River Delta of China, *Atmos. Chem. Phys.*, 22, 4355-4374, 10.5194/acp-22-4355-2022, 2022.
- Zhai, S. X., Jacob, D. J., Wang, X., Liu, Z., Wen, T., Shah, V., Li, K., Moch, J. M., Bates, K. H., Song, S., Shen, L., Zhang, Y., Luo, G., Yu, F., Sun, Y., Wang, L., Qi, M., Tao, J., Gui, K., Xu, H., Zhang, Q., Zhao, T., Wang, Y., Lee, H. C., Choi, H., and Liao, H.: Control of particulate nitrate air pollution in China, *Nat. Geosci.*, 14, 389-395, 10.1038/s41561-021-00726-z, 2021.
- 820 Zhang, Y.-L., Zhang, W., Fan, M.-Y., Li, J., Fang, H., Cao, F., Lin, Y.-C., Wilkins, B. P., Liu, X., Bao, M., Hong, Y., and Michalski, G.: A diurnal story of $\Delta^{17}\text{O}(\text{NO}_3^-)$ in urban Nanjing and its implication for nitrate aerosol formation, *npj Climate and Atmospheric Science*, 5, 50, 10.1038/s41612-022-00273-3, 2022.
- 825 Zhang, Z., Cao, L., Liang, Y., Guo, W., Guan, H., and Zheng, N.: Importance of NO₃ radical in particulate nitrate formation in a southeast Chinese urban city: New constraints by $\delta^{15}\text{N}$ - $\delta^{18}\text{O}$ space of NO₃, *Atmos. Environ.*, 253, 118387, <https://doi.org/10.1016/j.atmosenv.2021.118387>, 2021.
- 830 Zheng, B., Zhang, Q., Zhang, Y., He, K. B., Wang, K., Zheng, G. J., Duan, F. K., Ma, Y. L., and Kimoto, T.: Heterogeneous chemistry: A mechanism missing in current models to explain secondary inorganic aerosol formation during the January 2013 haze episode in North China, *Atmos. Chem. Phys.*, 15, 2031-2049, 10.5194/acp-15-2031-2015, 2015.
- 835 Zheng, B., Tong, D., Li, M., Liu, F., Hong, C., Geng, G., Li, H., Li, X., Peng, L., Qi, J., Yan, L., Zhang, Y., Zhao, H., Zheng, Y., He, K., and Zhang, Q.: Trends in China's anthropogenic emissions since 2010 as the consequence of clean air actions, *Atmos. Chem. Phys.*, 18, 14095-14111, 10.5194/acp-18-14095-2018, 2018.
- Zheng, H., Song, S., Sarwar, G., Gen, M., Wang, S., Ding, D., Chang, X., Zhang, S., Xing, J., Sun, Y., Ji, D., Chan, C. K., Gao, J., and McElroy, M. B.: Contribution of Particulate Nitrate Photolysis to Heterogeneous Sulfate Formation for Winter Haze in China, *Environ. Sci. Technol. Lett.*, 7, 632-638, 10.1021/acs.estlett.0c00368, 2020.
- 840 Zhou, M., Nie, W., Qiao, L., Huang, D. D., Zhu, S., Lou, S., Wang, H., Wang, Q., Tao, S., Sun, P., Liu, Y., Xu, Z., An, J., Yan, R., Su, H., Huang, C., Ding, A., and Chen, C.: Elevated formation of particulate nitrate from N₂O₅ hydrolysis in the Yangtze River Delta region from 2011 to 2019, *Geophys. Res. Lett.*, n/a, e2021GL097393, <https://doi.org/10.1029/2021GL097393>, 2022.

845

Tables and Figures

Table 1. Model performance for meteorological parameters for January, April, July, October and the annual average of 2017 in the entire YRD region. The values that do not meet the criteria are denoted in bold.

Parameters	Statistic(benchmarks)	January	April	July	October	Annual
T2(°C)	MB ($\leq \pm 0.5$)	1.56	1.04	0.67	1.98	1.31
	RMSE	1.99	1.76	1.57	2.24	1.89
	IOA (≥ 0.8)	0.89	0.93	0.85	0.89	0.89
	R	0.94	0.93	0.85	0.95	0.92
RH(%)	MB	-6.96	-10.70	-9.06	-5.98	-8.17
	RMSE	9.73	13.14	10.91	8.02	10.45
	IOA	0.88	0.83	0.72	0.82	0.81
	R	0.90	0.91	0.88	0.87	0.89
WD(°)	MB ($\leq \pm 10$)	-12.78	-0.92	12.26	-24.42	-6.46
	RMSE	37.68	36.04	26.61	55.85	39.05
	IOA	0.88	0.89	0.88	0.76	0.85
	R	0.85	0.82	0.85	0.70	0.81
WS(m/s)	MB ($\leq \pm 0.5$)	0.61	0.76	1.03	0.69	0.77
	RMSE (≤ 2.0)	0.82	1.06	1.31	0.96	1.04
	IOA (≥ 0.6)	0.84	0.71	0.65	0.82	0.76
	R	0.89	0.75	0.75	0.88	0.82

850 Notes: The following equations of MB, RMSE and IOA are defined in Table S4. The benchmarks are suggested by Emery and Tai (2001).

852 **Table 2.** Model performance of major pollutants for the full year of 2017 in five representative YRD cities ^a.

^b Pollutants	Shanghai				Nanjing				Hefei				Hangzhou				Changzhou			
	^c NMB	NME	MB	R	NMB	NME	MB	R	NMB	NME	MB	R	NMB	NME	MB	R	NMB	NME	MB	R
MDA8 O ₃	-0.01	0.20	-1.07	0.88	0.17	0.28	18.59	0.76	0.17	0.24	17.23	0.81	0.25	0.31	26.60	0.80	0.19	0.26	19.85	0.84
NO ₂	-0.05	0.23	-1.89	0.71	-0.07	0.26	-3.20	0.50	-0.11	0.26	-5.21	0.67	-0.25	0.34	-10.37	0.51	-0.07	0.24	-2.67	0.56
SO ₂	-0.38	0.43	-4.61	0.66	0.12	0.45	1.83	0.32	0.01	0.36	0.18	0.75	-0.28	0.40	-3.15	0.46	0.09	0.34	1.54	0.48
CO	-0.38	0.40	-0.29	0.67	-0.17	0.33	-0.17	0.45	-0.22	0.26	-0.19	0.76	-0.30	0.34	-0.25	0.55	0.06	0.25	0.05	0.64
PM _{2.5}	-0.08	0.30	-2.80	0.73	0.28	0.44	10.29	0.75	0.41	0.51	21.42	0.76	0.05	0.31	1.88	0.69	0.25	0.37	10.59	0.78
NO ₃ ⁻	-0.49	0.63	-3.25	0.70					0.07	0.65	0.32	0.59	0.11	0.79	0.64	0.43	-0.36	0.58	-3.34	0.56

853 Notes: ^a The year of 2017 includes the four typical months (January, April, July, and October). ^b MDA8 O₃, NO₂, SO₂ and PM_{2.5} units (μg/m³), CO units (mg/m³).

854 ^c The equations of NMB, NME, MB and R are found in Table S4. The values that do not meet the criteria are highlighted in bold.

855 The recommended benchmarks for MDA8 O₃, 24-h PM_{2.5} and NO₃⁻ are suggested by Emery et al. (2017) and Huang et al. (2021). [_____](#)

856 | 

857 **Table 3.** ~~Model performance for~~ Seasonal TNO₃ production rates (ppb/h) and ~~daily contributions in percentage(%)~~ of the major production
 858 pathways ~~(%) for the four seasons of 2017~~ in five representative YRD-cities.

Selected cities	Seasons	TNO ₃	OH NO ₂	HET N ₂ O ₅	OH NO ₂ (%)	HET N ₂ O ₅ (%)	Others (%)
Shanghai	Winter	0.31 ±0.13	0.21 ±0.18	0.09 ±0.06	69.3%	28.4%	2.2%
	Spring	0.65 ±0.35	0.52 ±0.43	0.10 ±0.09	81.8%	15.3%	2.9%
	Summer	1.09 ±0.68	0.90 ±0.80	0.13 ±0.15	82.9%	12.2%	4.9%
	Autumn	0.28 ±0.22	0.24 ±0.24	0.03 ±0.03	86.9%	11.1%	2.0%
Nanjing	Winter	0.38 ±0.13	0.23 ±0.20	0.14 ±0.11	59.2%	36.1%	4.7%
	Spring	0.65 ±0.29	0.48 ±0.40	0.14 ±0.12	73.1%	21.4%	5.4%
	Summer	0.83 ±0.41	0.62 ±0.55	0.15 ±0.17	74.7%	17.9%	7.4%
	Autumn	0.50 ±0.25	0.35 ±0.32	0.13 ±0.11	69.7%	25.4%	4.9%
Hefei	Winter	0.38 ±0.13	0.26 ±0.18	0.10 ±0.07	66.9%	27.1%	6.0%
	Spring	0.63 ±0.24	0.49 ±0.30	0.10 ±0.09	78.5%	16.5%	5.0%
	Summer	0.66 ±0.26	0.54 ±0.30	0.07 ±0.08	81.7%	10.4%	7.9%
	Autumn	0.48 ±0.18	0.35 ±0.24	0.11 ±0.08	72.5%	21.8%	5.7%
Changzhou	Winter	0.41 ±0.15	0.29 ±0.20	0.11 ±0.08	68.9%	26.8%	4.3%
	Spring	0.64 ±0.25	0.48 ±0.31	0.13 ±0.12	74.9%	20.9%	4.2%
	Summer	0.70 ±0.27	0.55 ±0.31	0.10 ±0.13	78.7%	14.3%	7.0%
	Autumn	0.46 ±0.19	0.36 ±0.24	0.08 ±0.07	77.6%	18.3%	4.1%
Hangzhou	Winter	0.43 ±0.15	0.26 ±0.21	0.15 ±0.12	59.7%	35.5%	4.8%
	Spring	0.57 ±0.24	0.40 ±0.33	0.13 ±0.12	70.5%	23.3%	6.2%
	Summer	0.47 ±0.23	0.36 ±0.29	0.05 ±0.05	76.4%	10.7%	12.9%
	Autumn	0.46 ±0.26	0.34 ±0.32	0.10 ±0.09	73.8%	21.3%	4.9%

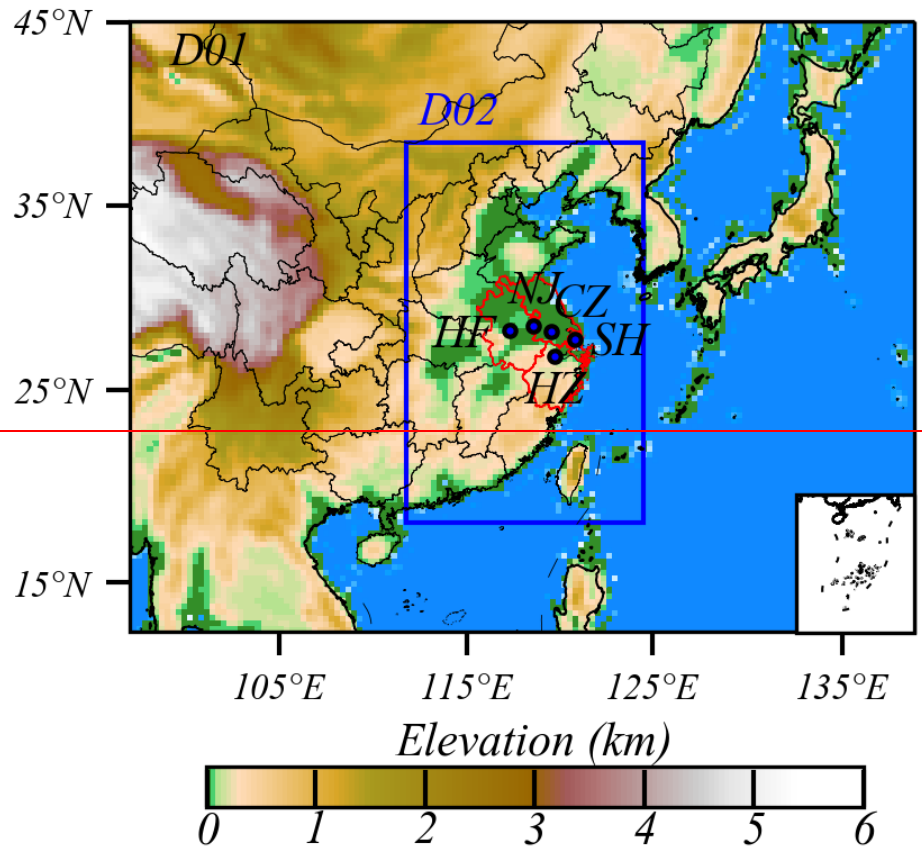
859

860 **Table 4.** Comparison of contributions of major nitrate formation pathways in China and others regions ^a.

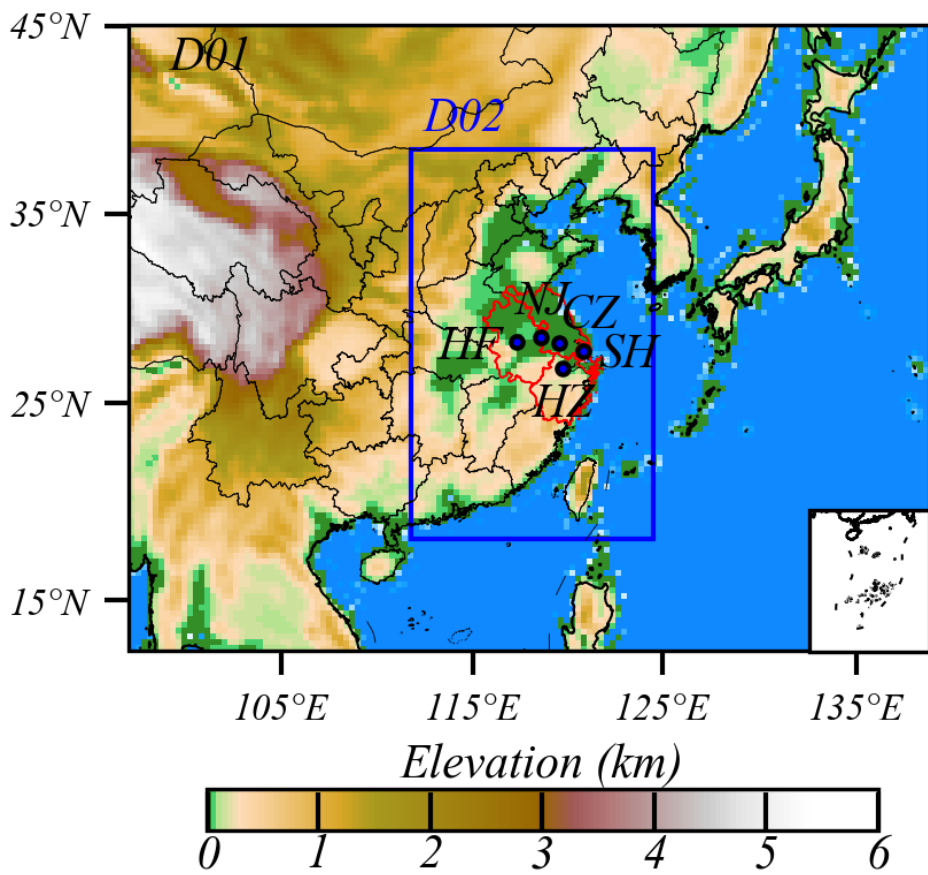
References	Methods ^b	Study seasons	Year	Study regions	NO ₃ ⁻ formation pathways ^c	Time metric	Contribution (%)
(Li et al., 2021b)	WRF-Chem	Warm (Aug –Sep)	2016	NCP, YRD	OH+NO ₂ (layer 1)	season-mean	60-92%
		Cold (Nov-Dec)			HET N ₂ O ₅ (layer 1)		8-40%
(Qu et al., 2021)	WRF-CMAQ PA	Transition season (Oct-Dec)	2015	PRD	OH+NO ₂ (layers 1-4)	day-mean	92-96%
					HET N ₂ O ₅ (layers 1-4)	night- mean	64-72%
(Chuang et al., 2022)	WRF-CMAQ PA	Transition season (Mar - Apr)	2017	Taiwan	OH+NO ₂	day-mean	> 90%
					HET N ₂ O ₅	night- mean	30-90%
(Wu et al., 2021)	WRF-Chem; Nitrogen Isotopes	Cold (Dec-Jan)	2017	Xi'an	HET N ₂ O ₅ (surface)	season-mean	13-35 %
(Chan et al., 2021)	GEOS-Chem; Isotope tracing	Cold	2014-15	NCP	OH+NO ₂ &HET N ₂ O ₅ (surface)	season-mean	34 % & 45 %
(Fu et al., 2020)	WRF-CMAQ PA	Cold (Dec)	2017	NCP	OH+NO ₂ (HET N ₂ O ₅) 10 layers	season-mean	43% (44%)
(Liu et al., 2020a)	WRF-Chem	Cold (Dec)	2016	NCP	HET N ₂ O ₅ (surface)	haze-mean	52 %
					HET N ₂ O ₅ (PBL)	night (day)	83% (10%)
(Zhang et al., 2022)	Nitrogen &Oxygen Isotopes	Cold (Jan)	2017-18	Nanjing	OH+NO ₂ & HET N ₂ O ₅ (surface)	season-peak	48% & 72%
(Zhang et al., 2021)	Nitrogen &Oxygen Isotopes	Cold (Nov-Jan)	2017-18	Nanchang	HET N ₂ O ₅ (surface)	season-mean	60%
(Fan et al., 2021)	Nitrogen &Oxygen Isotopes	Warm and Cold	2016-17	Beijing	OH+NO ₂ &HET N ₂ O ₅ (260 m)	Clean days	20% (80%)
(Luo et al., 2020a)	Nitrogen &Oxygen Isotopes	Spring(Mar-May)	2013	Beijing	OH+NO ₂ (surface)	Clean days	24-50%
					OH+NO ₂ (surface)	Polluted days	11-47%
(Luo et al., 2020b)	Nitrogen &Oxygen Isotopes	Four seasons	2018	Nanchang	OH+NO ₂ (HET N ₂ O ₅)	season-mean	12-59% (67-89%)
(Fan et al., 2020)	Nitrogen &Oxygen Isotopes	Cold (Nov-Dec)	2018	Beijing	HET N ₂ O ₅	haze period	64%
(He et al., 2020)	Nitrogen &Oxygen Isotopes	Warm and Cold season	2016	Shanghai	OH+NO ₂ (warm)	season-mean	84-92%
					OH+NO ₂ (cold)		48-74%
(Wang et al., 2019)	Nitrogen &Oxygen Isotopes	Warm and Cold season	2014	Beijing	OH+NO ₂	annual-mean	32 ± 10%
					HET N ₂ O ₅	annual-mean	68 ± 23%
(He et al., 2018)	Nitrogen isotopic	Cold (Oct-Jan)	2014	Beijing	HET N ₂ O ₅	night- haze	56-97 %
(Chen et al., 2020)	Field determination; Box model	Cold (Nov-Dec)	2016-17	Beijing	OH+NO ₂ & HET N ₂ O ₅ (240 m)	haze period	74-76% & 34%

(Sun et al., 2018)	Field determination; Box model	Cold (Nov-Dec)	2015	Nanjing	HET N ₂ O ₅ (surface)	haze period	80%
(Zang et al., 2022)	Field observations; Box model	Cold (Dec-Feb)	2018-19	Shanghai (urban & suburban areas)	OH+NO ₂ &HET N ₂ O ₅ (surface)	haze period	69% & 29%
(Womack et al., 2019)	Box model	Cold (Dec)	2016-17	Salt Lake Valley	HET N ₂ O ₅ (RL)	season-mean	43%
(Vrekoussis et al., 2004)	Field determination, Box model	Summer(Jul-Aug)	2001	South-East Europe	HET N ₂ O ₅ (surface)	season-mean	21%
(Kim et al., 2014)	WRF-CMAQ PA	Cold (Dec)	2009	The Great Lakes	OH+NO ₂ &HET N ₂ O ₅ (surface)	season-mean	28% & 57%
(Shah et al., 2018)	GEOS-Chem	Cold (Feb-Mar)	2015	Eastern US	OH+NO ₂ &HET N ₂ O ₅ (surface)	season-mean	36% & 62%
(Alexander et al., 2020)	GEOS-Chem; Oxygen Isotopes	Four seasons	2000-15	Global	OH+NO ₂ (below 1 km)	annual-mean	41-42%
					HET N ₂ O ₅ (below 1 km)		28-41%

861 Notes: ^a The ~~above studies~~[24 peer-reviewed publications](#) are conducted in the major regions and megalopolises of China (the North China Plain (NCP), Yangtze
862 River Delta (YRD), Pearl River Delta (PRD)), the United States, and the Global region. The comparison serves to quantify the relative contribution of two main
863 nitrate formation pathways in different seasons. ^b Methods include the 3-D CTMs, nitrogen and oxygen isotopes analysis, field determination, and box model. ^c
864 Surface represents the surface layer.

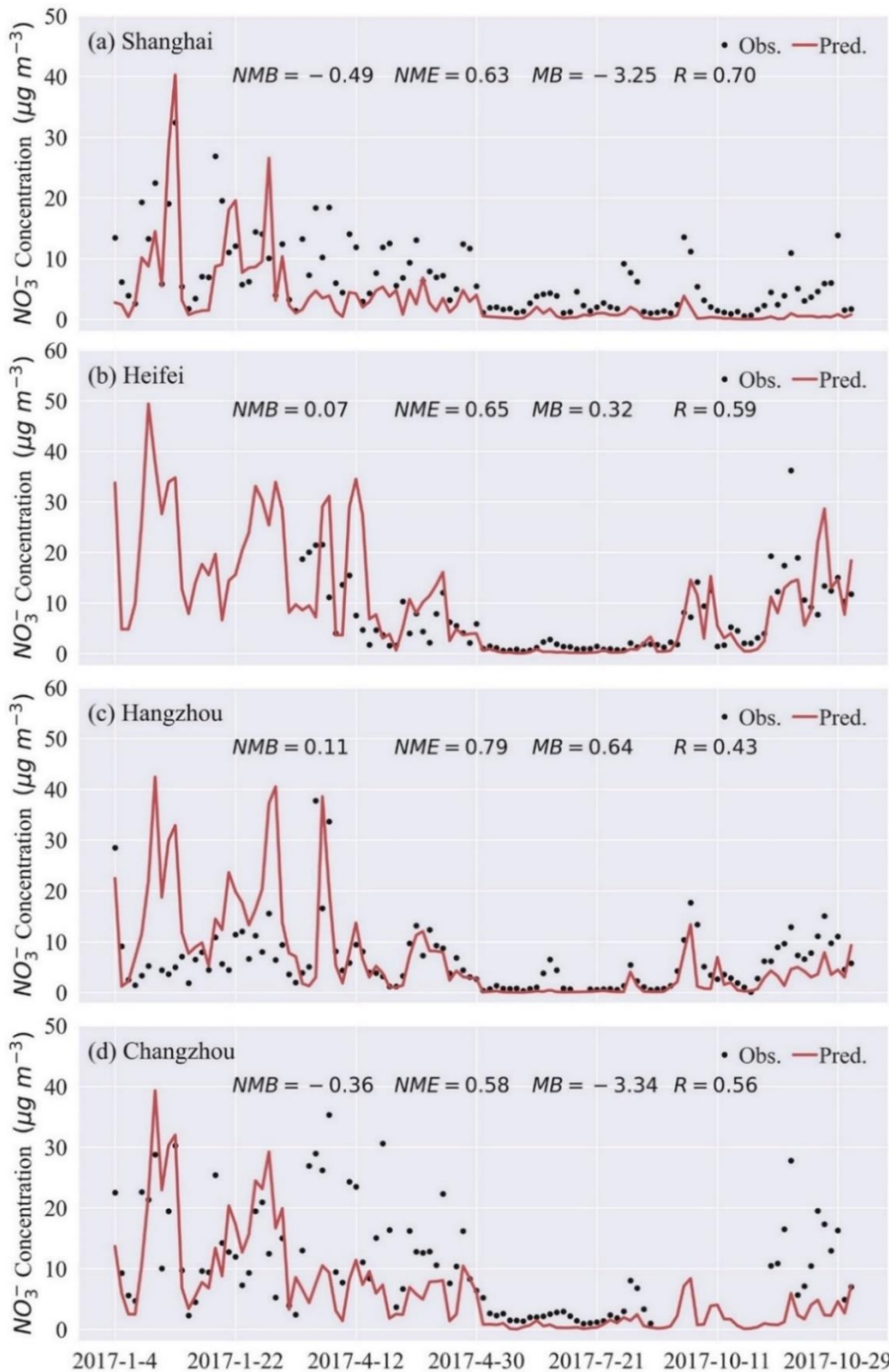


865

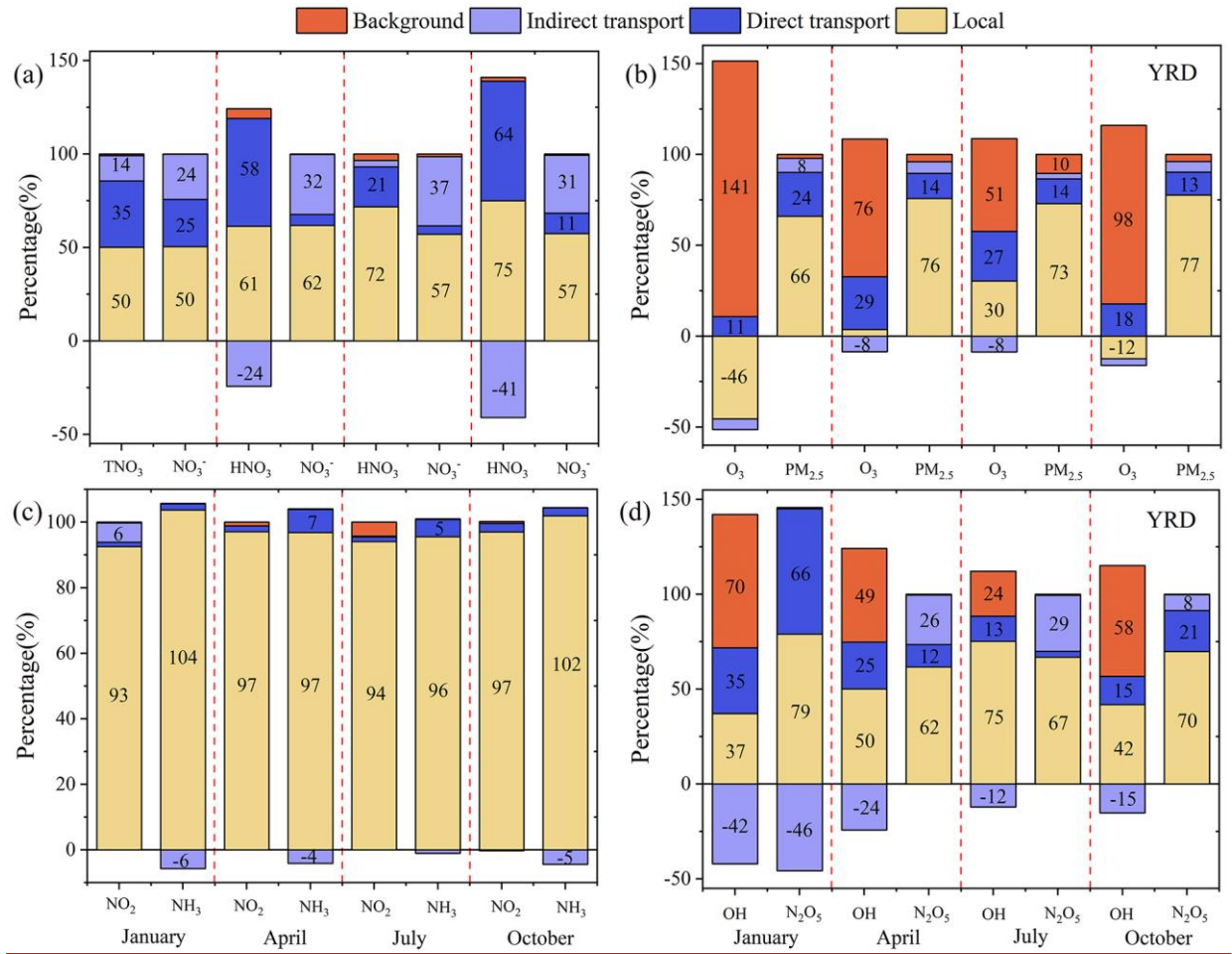


866

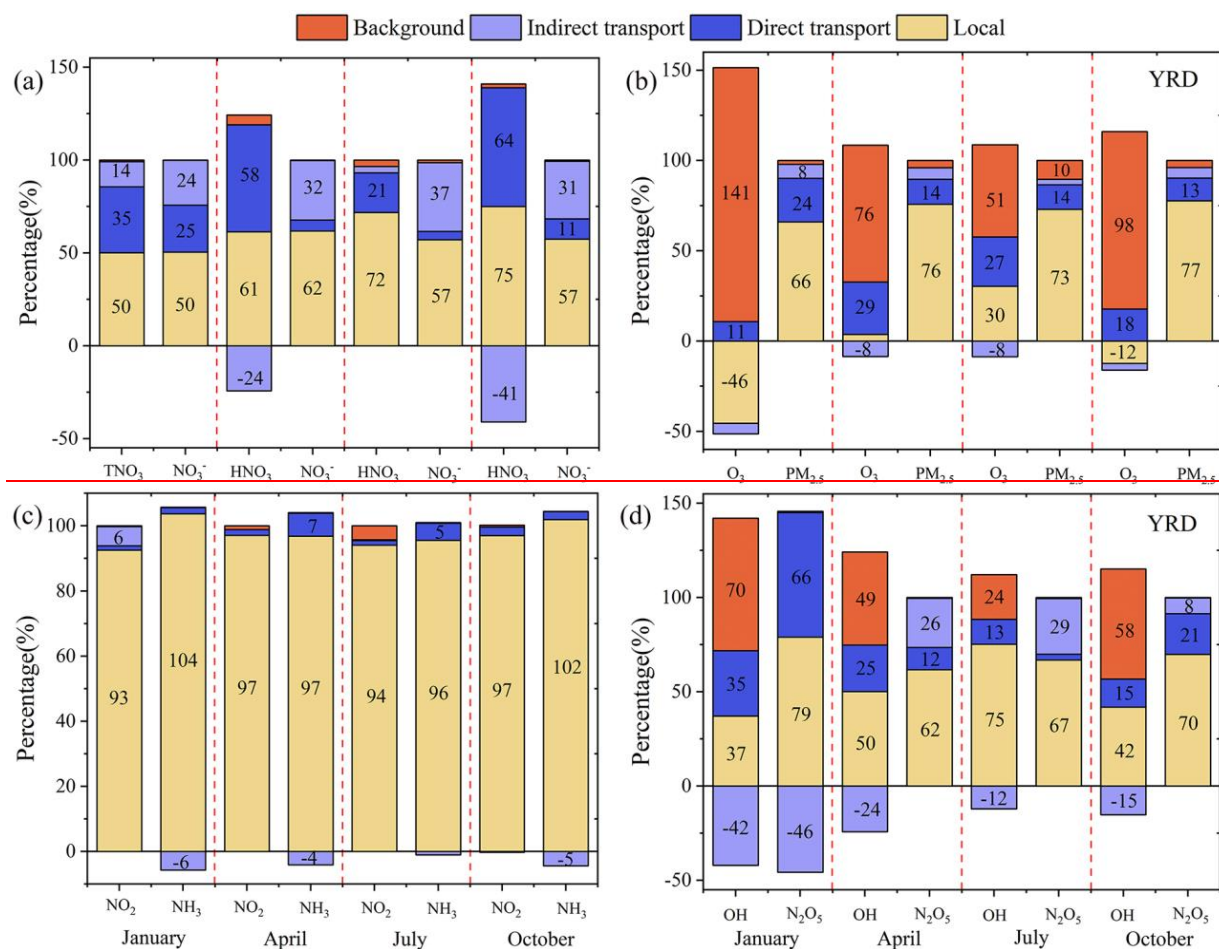
867 **Fig 1.** Entire YRD region as the target region (marked as red) in two nested
 868 simulation domains (36 and 12 km resolutions), and location of five representative
 869 YRD cities used in modeling evaluations in the d02 modeling domain.



870
 871 **Fig 2.** Time series of predicted (red) and observed (black) daily NO_3^- concentrations
 872 in four atmospheric environment supersites (a–d) in January, April, July, and October
 873 2017.



874

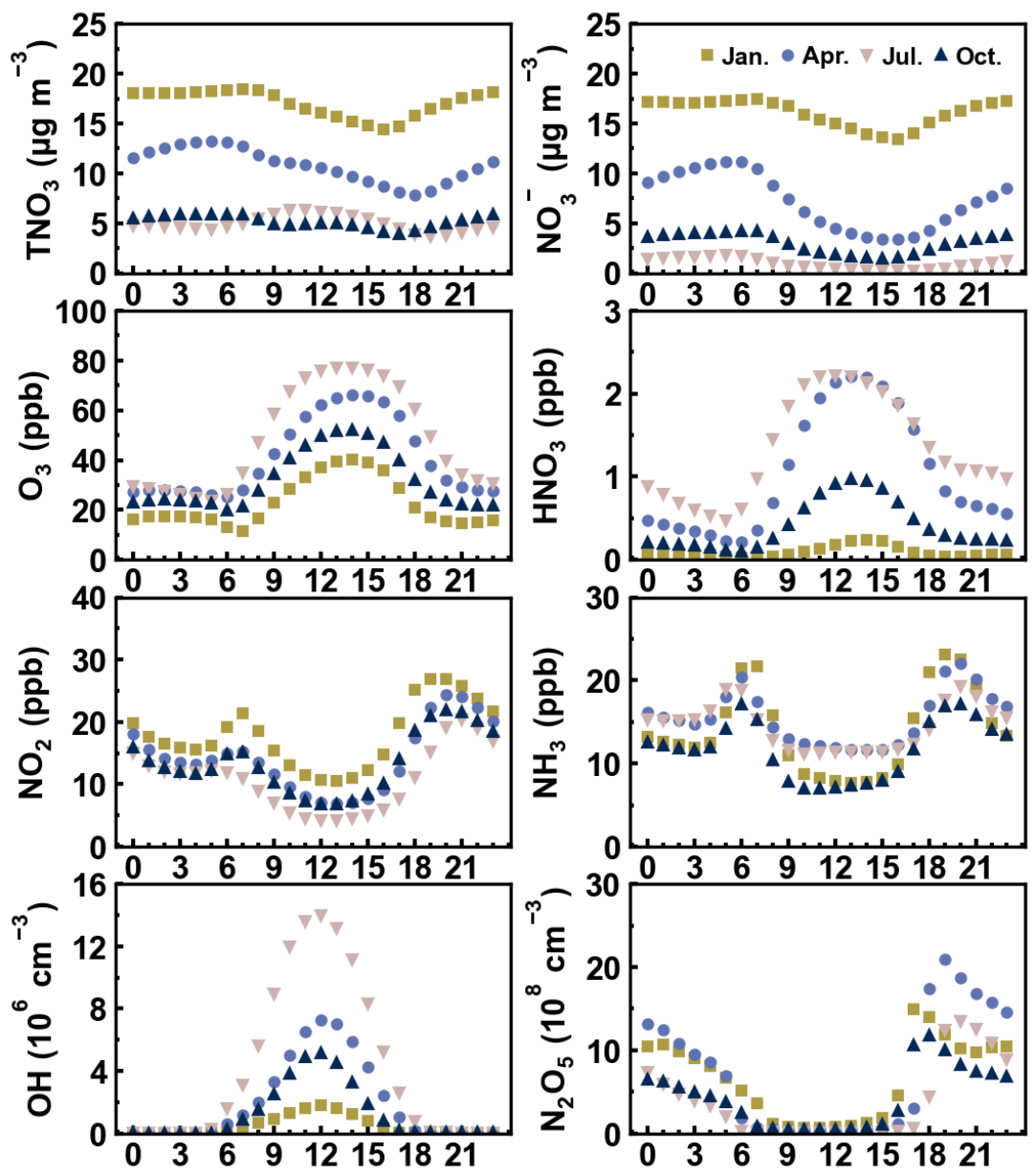


875

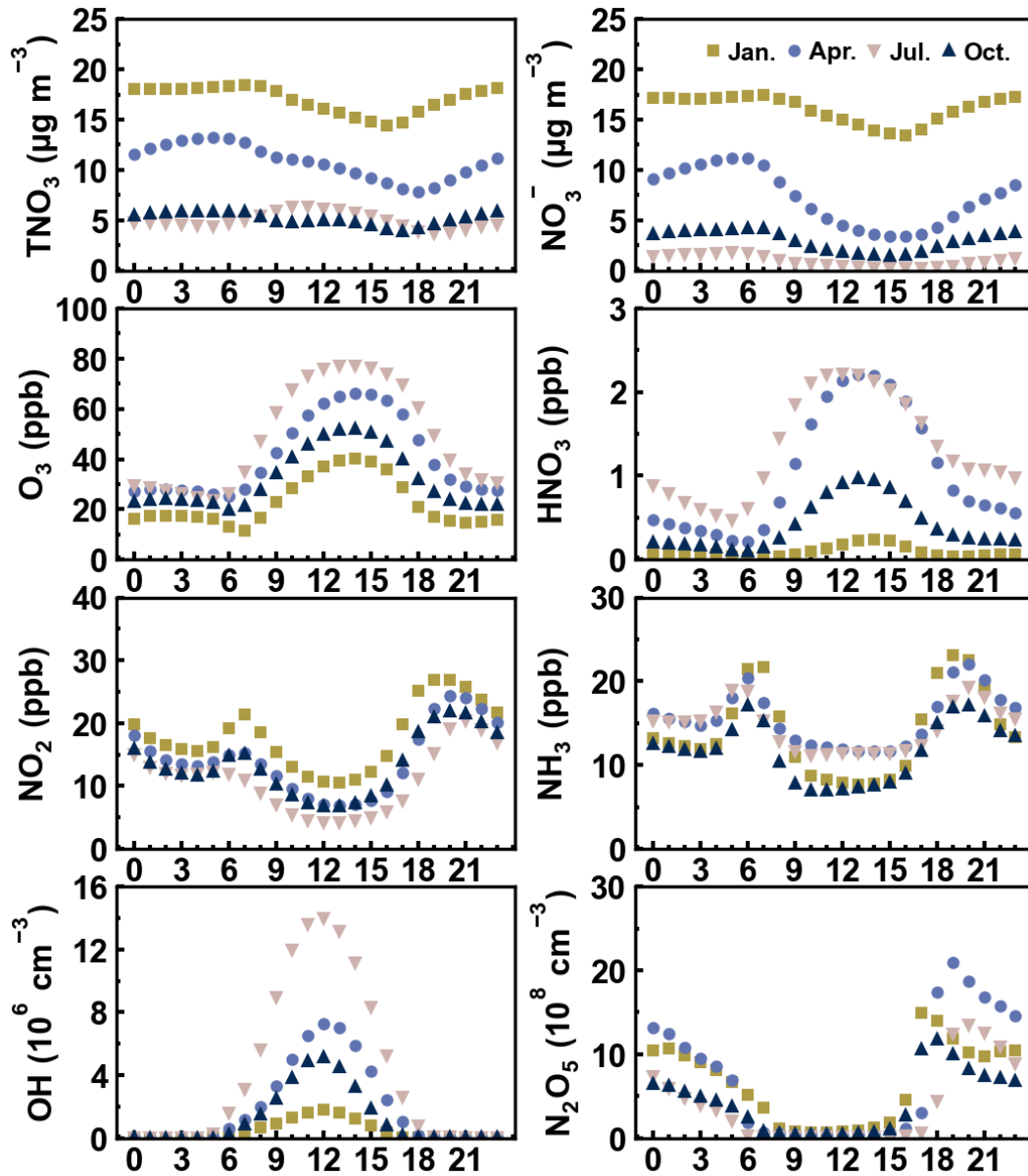
876 **Fig 3.** (a–d) Contributions of Background, Local, Indirect, and Direct transport to
 877 nitrate-related species in four months of 2017 for the entire YRD region.

878 Notes: Nitrate-related species represent NO₃⁻, HNO₃, PM_{2.5}, O₃, NO₂, NH₃, OH, and N₂O₅. The
 879 contributions of HNO₃ in January 2017 are shown in Fig. S6.

880 |



881

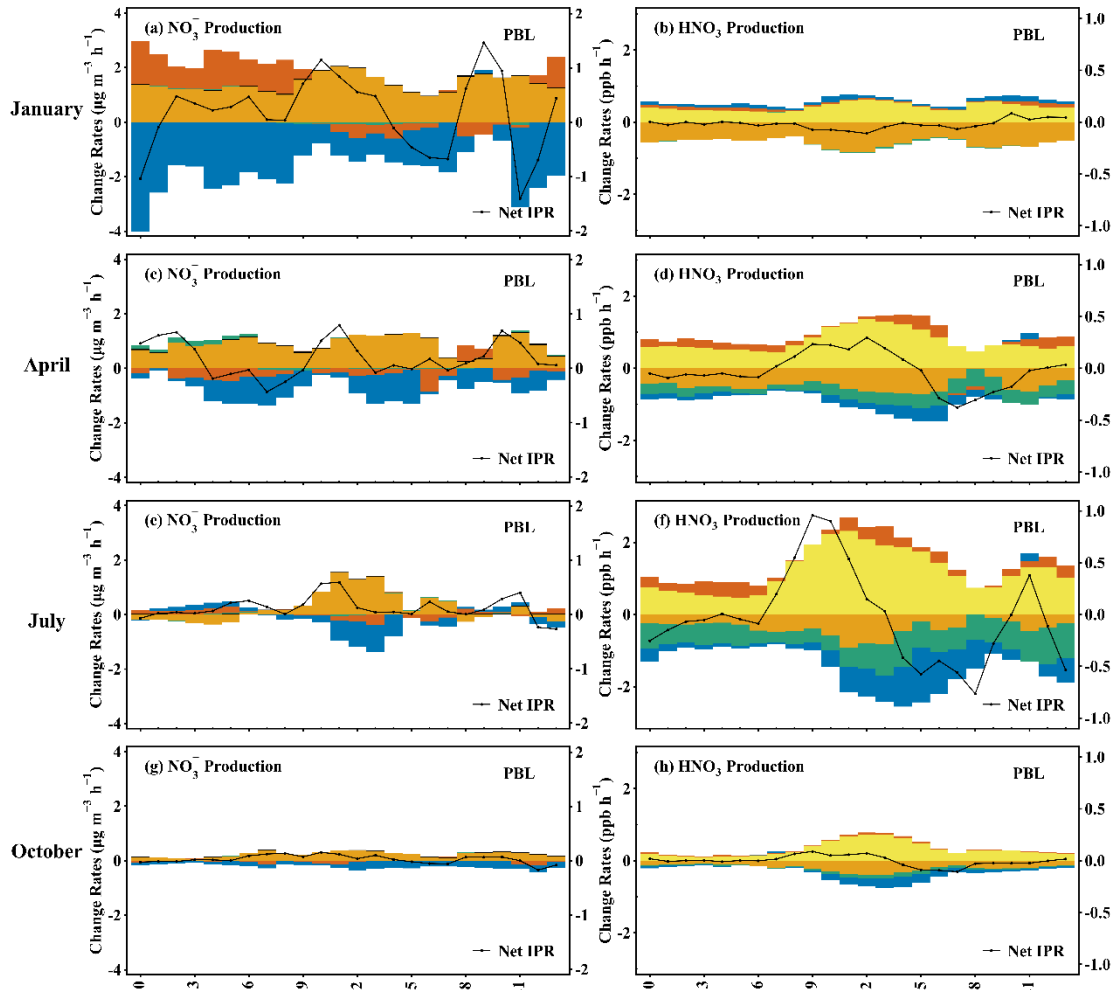


882

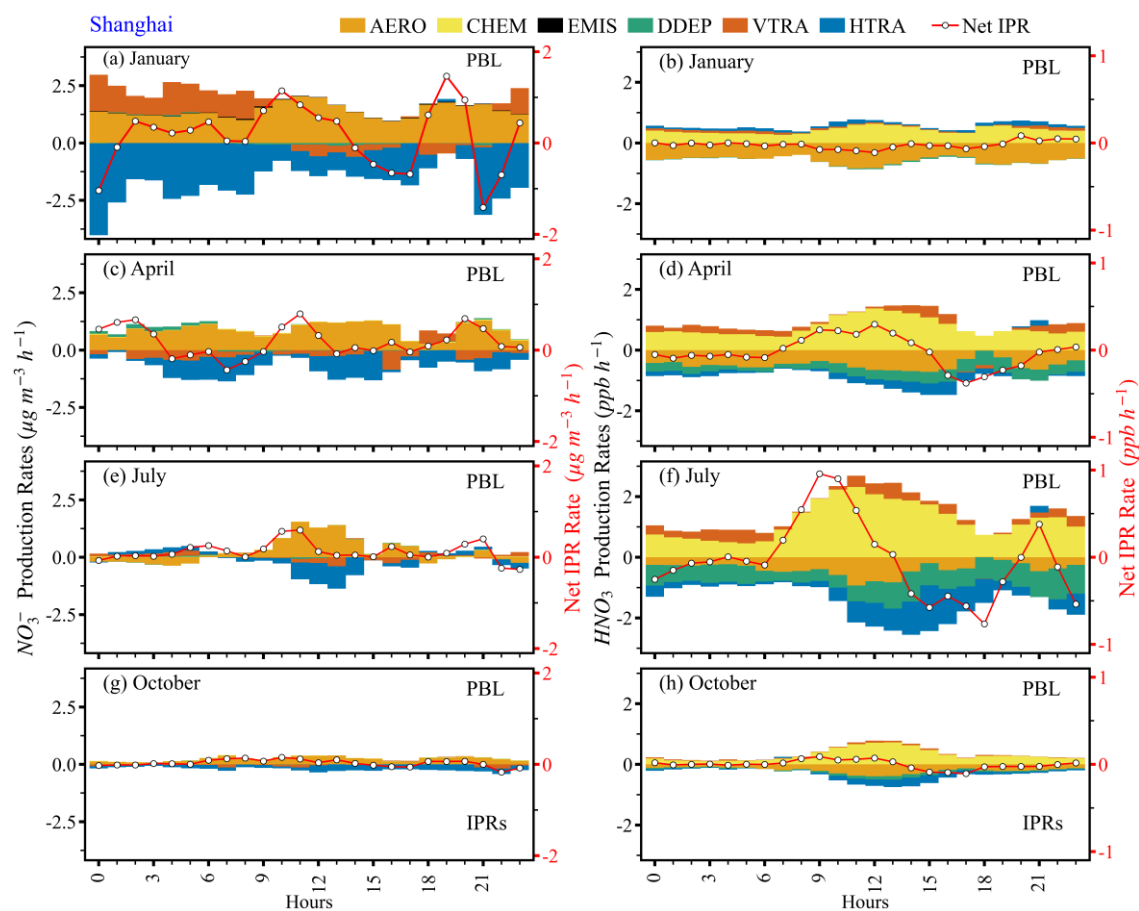
883 **Fig 4.** Monthly diurnal variations of three nitrate-phases (NO_3^- , HNO_3 , and TNO_3),
 884 the major nitrate-precursors (O_3 , NO_2 , NH_3 , and $\text{NH}_3\text{N}_2\text{O}_5$) and major-atmospheric
 885 oxidants (OH and N_2O_5) for the entire YRD region under the base scenario. The
 886 X axis marks each hour of the day (Beijing time).

IPRs

AERO CHEM EMIS DDEP VTRA HTRA



887



888

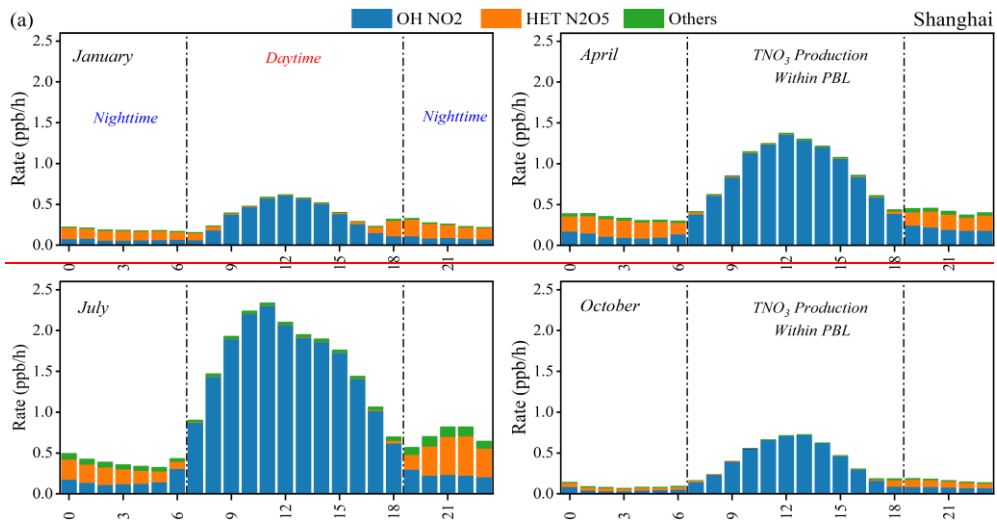
889

890

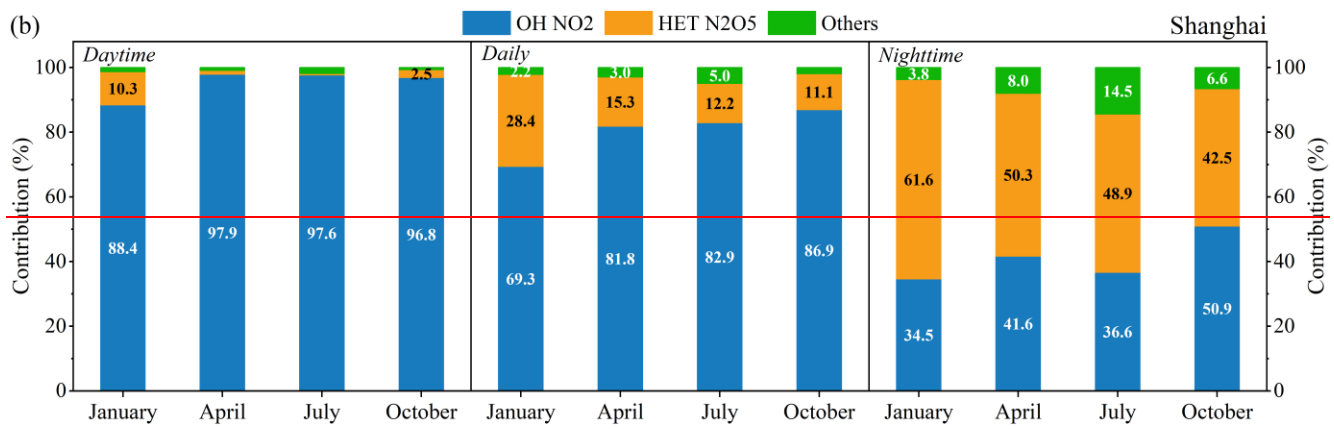
891

Fig 5. Diel variations in physical and chemical processes rates of NO_3^- and HNO_3 production (a–h) within the PBL in Shanghai. ~~Black~~Red line represents the net IPR value for each hour of the day; its value scale is on the right Y axis.

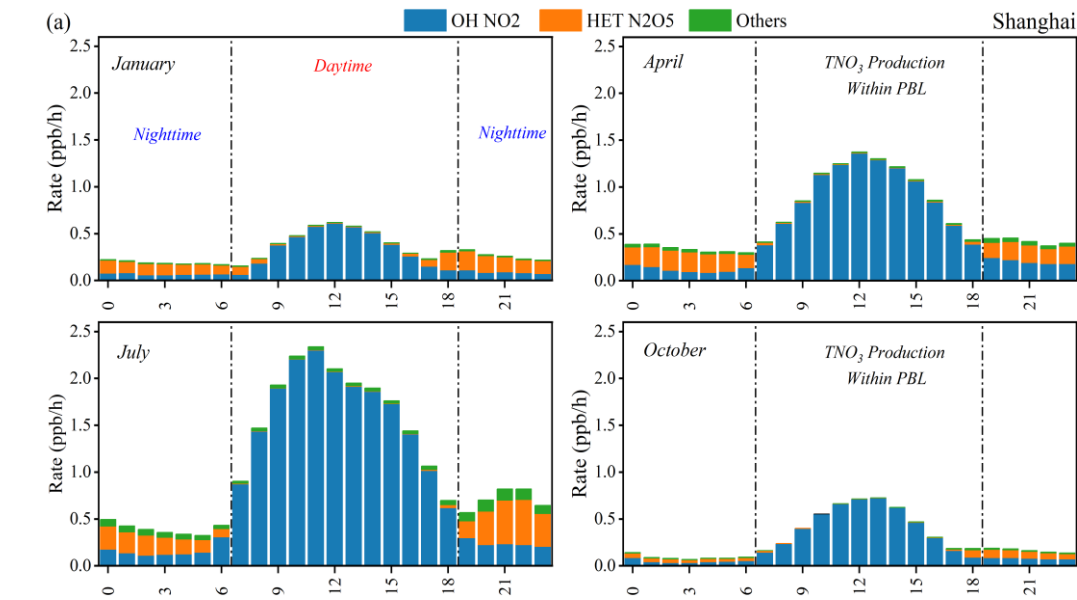
892

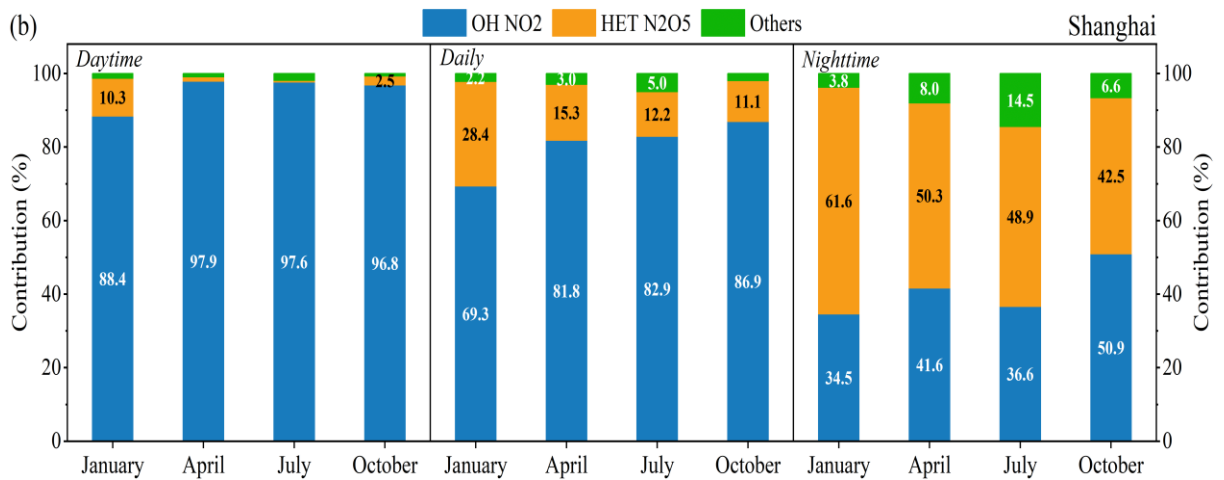


893



894

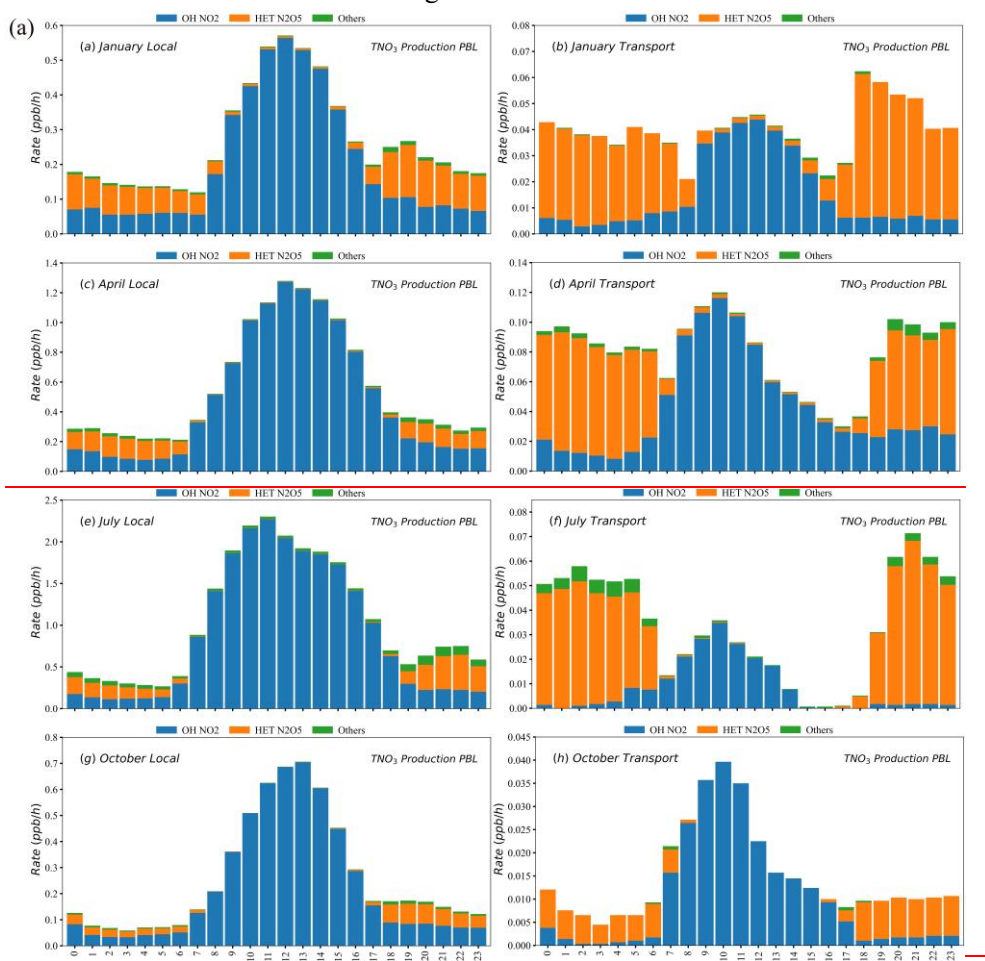




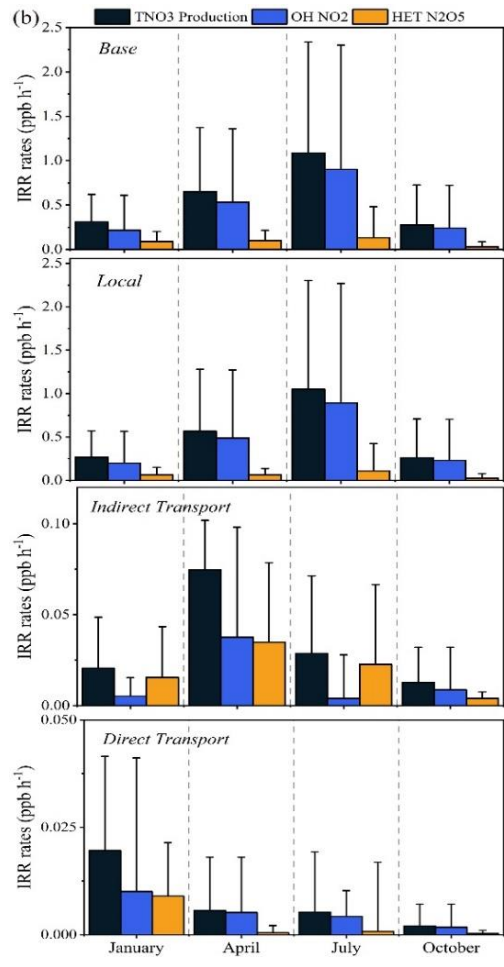
895

896 **Fig 6.** (a) Mean diurnal variations of TNO₃ production rates in different pathways in
 897 2017 in Shanghai. (b) Average potential contribution of OH + NO₂, HET N₂O₅ and
 898 Others pathways to TNO₃ chemical production in Shanghai within the PBL under
 899 base case simulation.

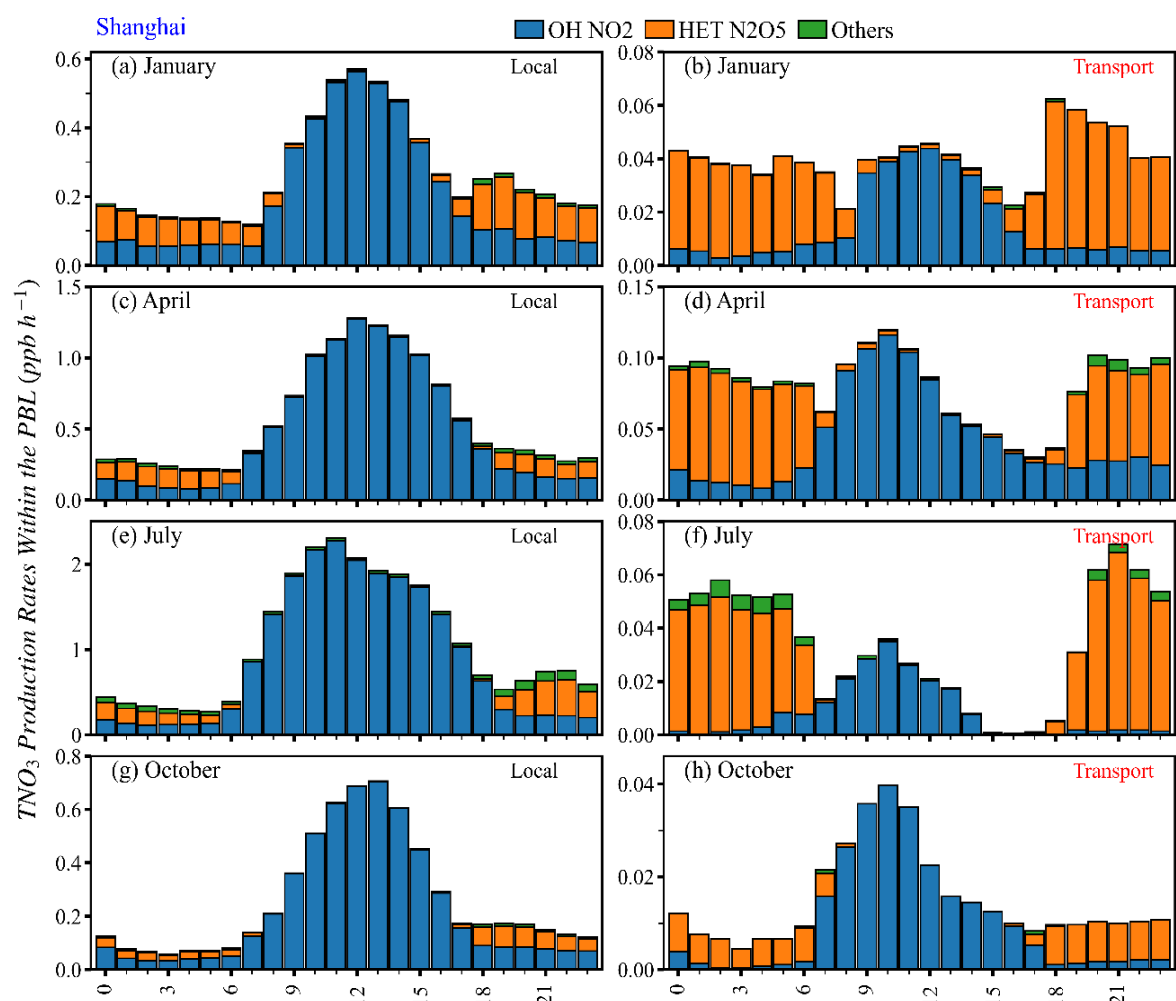
900 Notes: Daytime (7:00–18:00), Nighttime (19:00–6:00). OH + NO₂ and HET N₂O₅ pathways are
 901 noted as “OH NO₂” and “HET N₂O₅” in Figs.6 and 7.



902

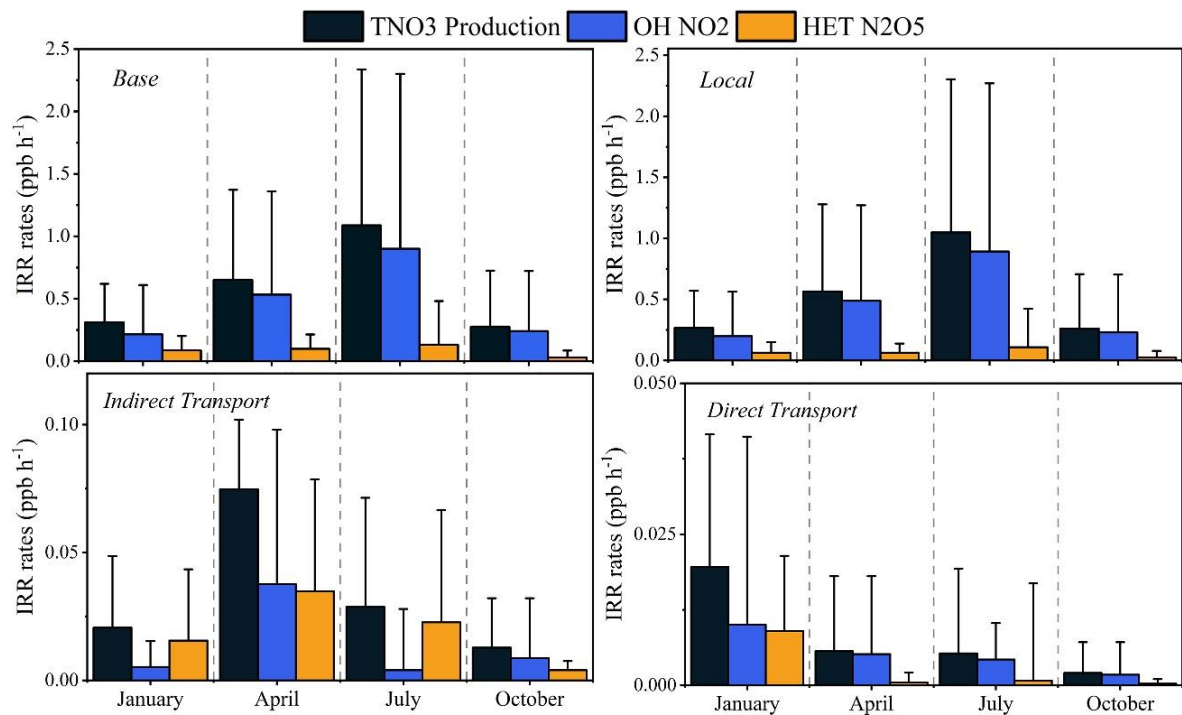


903



904

905 **Fig 7.** (a) Mean diurnal variations of TNO₃ production rates in major pathways from
 906 the local and transport (sum of indirect and direct transport) contributions. (b) Total
 907 IRRs
 908



909

910 **Fig 8.** The seasonal rates of TNO_3^- production and the major pathways in the
 911 base case, and from the local and transport contributions within the PBL. The error
 912 bar indicates one standard deviation.